6

Uniform Flow and Flow Resistance

6.0 Introduction and Overview

The central problem of open-channel-flow hydraulics can be stated as follows: Given a channel reach with a specified geometry, material, and slope, what are the relations among flow depth, average velocity, width, and discharge? Solutions to this problem are essential for solving important practical problems, including 1) the design of channels and canals, 2) the areal extent of flooding that will result from a storm or snowmelt event, 3) the rate of travel of a flood wave through a channel network, and 4) the size and quantity of material that can be eroded or transported by various flows.

The characterization of flow resistance (defined precisely in section 6.4) is essential to the solutions of this central problem, because it provides the relation between velocity (usually considered the dependent variable) and 1) specified geometric and boundary characteristics of the channel, usually considered to be essentially constant; and 2) the flow magnitude expressed as discharge or depth, considered as the independent variable that may change with time in a given reach.

The definition of flow resistance is developed from the concepts of uniform flow (section 4.2.1.2) and force balance (section 4.7). Recall that in a steady uniform flow, there is no acceleration; thus, by Newton's second law of motion, there is no net force acting on the fluid. Although uniform flow is an ideal state seldom strictly achieved in natural flows, it is often a valid assumption because open-channel flows are self-adjusting dynamic systems (negative feedback loops) that are always tending toward a balance of driving and resisting forces: an increase (decrease) in velocity produces an increase (decrease) in resistance tending to decrease (increase) velocity.

To better appreciate the basic concepts underlying the definition and determination of resistance, this chapter begins by reviewing the basic geometric features of river reaches and reach boundaries presented in section 2.3. We then adapt the definition of uniform flow as applied to a fluid element to apply to a typical river reach and derive the Chézy equation, which is the basic equation for macroscopic uniform flows. This derivation allows us to formulate a simple definition of resistance. We then undertake an examination of the factors that determine flow resistance; this examination involves applying the principles of dimensional analysis developed in section 4.8.2 and the velocity-profile relations derived in chapter 5. The chapter concludes by exploring resistance in nonuniform flows and practical approaches to determining resistance in natural channels.

As we will see, there is still much research to be done to advance our understanding of resistance in natural rivers.

6.1 Boundary Characteristics

As noted above, the nature as well as the shape of the channel boundary affects flow resistance. The classification of boundary characteristics in figure 2.15 provides perspective for the discussion in the remainder of this chapter: Most of the analytical relations that have been developed and experimental results that have been obtained are for rigid, impervious, nonalluvial or plane-bed alluvial boundaries, while many, if not most, natural channels fall into other categories.

In this chapter, we consider cross-section-averaged or reach-averaged conditions rather than local "vertically" averaged velocities (U_w) and local depths (Y_w), and will designate these larger scale averages as U and Y, respectively. Figure 6.1 shows the spatial scales typically associated with these terms. Since our analytical reasoning will be based on the assumption of prismatic channels, there is no distinction between cross-section averaging and reach averaging. We will often invoke the wide

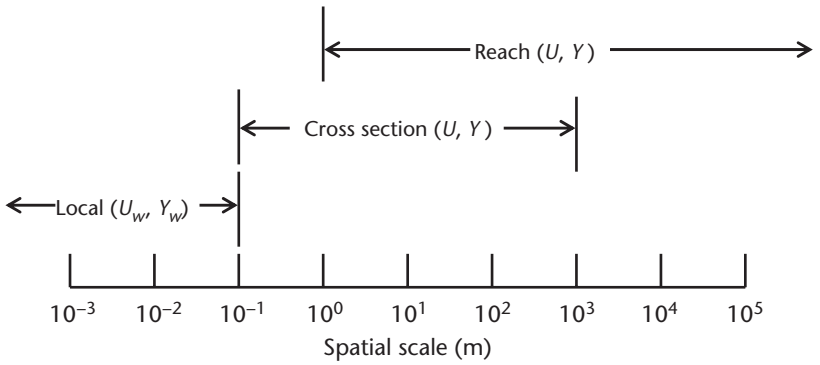

Figure 6.1 Spatial scales typically associated with local, cross-section-averaged, and reach-averaged velocities, depths, and resistance. After Yen (2002).

open-channel concept to justify applying the local, two-dimensional "vertical" velocity distributions discussed in chapter 5 [especially the Prandtl-von Kármán (P-vK) law] to entire cross sections.

We saw in section 5.3.1.6 that channel boundaries can be hydraulically "smooth" or "rough" depending on whether the boundary Reynolds number Re_b is greater or less than 5, where

$$Re_b \equiv \frac{u_* \cdot y_r}{\nu} \tag{6.1}$$

u_* is shear velocity, ν is kinematic viscosity, and y_r is the **roughness height**, that is, the characteristic height of roughness elements (projections) on the boundary (see figure 5.7). In natural alluvial channels, the bed material usually consists of sediment grains with a range of diameters (figure 2.17a). For a particular reach the characteristic height y_r is usually determined as shown in figure 2.17b:

$$y_r = k_r \cdot d_p, \tag{6.2}$$

where d_p is the diameter of particles larger than p percent of the particles on the boundary surface and k_r is a multiplier ≥ 1. Different investigators have used different values for p and k_r (see Chang 1988, p. 50); we will generally assume $k_r = 1$ and $p = 84$ so that $y_r = d_{84}$.

Of course, other aspects of the boundary affect the effective roughness height, especially the spacing and shape of particles. And, as suggested in figure 2.15, the appropriate value for y_r is affected by the presence of bedforms, growing and dead vegetation, and other factors.

6.2 Uniform Flow in Open Channels

6.2.1 Basic Definition

The concepts of steady flow and uniform flow were introduced in section 4.2.1.2 in the context of the movement of a fluid element in the x-direction along a streamline:

> If the element velocity u at a given point on a streamline does not change with time, the flow is **steady** (local acceleration $du/dt = 0$); otherwise, it is **unsteady**.
> If the element velocity at any instant is constant along a streamline, the flow is **uniform** (convective acceleration $du/dx = 0$); otherwise, it is **nonuniform**.

In the remainder of this text we will be concerned with the entirety of a flow within a reach of finite length rather than an individual fluid element flowing along a streamline. Furthermore, in turbulent flows, which include the great majority of natural open-channel flows, turbulent eddies preclude the existence of strictly steady or uniform flow. To account for these conditions we must modify the definition of "steady" and "uniform." To do this, we first designate the X-coordinate direction as the downstream direction for a reach and define U as the downstream-directed velocity,

1) time-averaged over a period longer than the time scale of turbulent fluctuations and 2) space-averaged over a cross section. Then,

- In **steady flow**, $dU/dt = 0$ at any cross section.
- In **uniform flow**, $dU/dX = 0$ at any instant.

As noted by Chow (1959, p. 89), unsteady uniform flow is virtually impossible of occurrence. Thus, henceforth, "uniform flow" implies "steady uniform flow." Note, however, that a nonuniform flow may be steady or unsteady.

We will usually assume that the discharge, Q, in a reach is constant in space and time, where

$$Q = W \cdot Y \cdot U, \tag{6.3}$$

W is the water-surface width, and Y is average depth.

In uniform flow with spatially constant Q, it must also be true that depth and width are constant, so "uniform flow" implies $dY/dX = 0$ and $dW/dX = 0$.[1] And, since the depth does not change, "uniform flow" implies that the water-surface slope is identical to the channel slope. Thus, it must also be true that for strictly uniform flow, cross-section shape is constant through a reach (i.e., the channel is prismatic).

Figure 6.2 further illustrates the concept of uniform flow. Here, a river or canal with constant channel slope θ_0, geometry, and bed and bank material, and no other inputs of water, connects two large reservoirs that maintain constant surface elevations. Under these conditions, the discharge will be constant along the entire channel. As the water leaves the upstream reservoir, it accelerates from zero velocity due to the downslope component of gravity, $g \cdot \sin\theta_s$, where θ_s is the local slope of the water surface. As it accelerates, the frictional resistance of the boundary is transmitted into the fluid by viscosity and turbulence (as in figure 3.28). This resistance increases as the velocity increases and soon balances the gravitational force,[2] at which point there is no further acceleration. Downstream of this point, the water-surface slope θ_s equals the channel slope θ_0, the cross-section-averaged velocity and depth become constant, and uniform flow is established. The velocity and depth remain constant

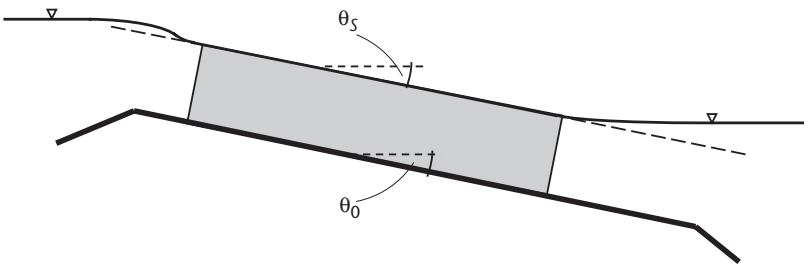

Figure 6.2 Idealized development of uniform flow in a channel of constant slope, θ_0, geometry, and bed material connecting two reservoirs. The shaded area is the region of uniform flow, where the downstream component of gravity is balanced by frictional resistance and the water-surface slope θ_S equals θ_0.

until the water-surface slope begins to decrease ($\theta_s < \theta_0$) to allow transition to the water level in the downstream reservoir, which is maintained at a level higher than that associated with uniform flow. This marks the beginning of negative acceleration and the downstream end of uniform flow.

6.2.2 Qualifications

Even with the above definitions, we see that strictly uniform flow is an idealization that cannot be attained in nonprismatic natural channels. And, even in prismatic channels there are hydraulic realities that usually prevent the attainment of truly uniform flow; these are described in the following subsections. Despite these realities, the concept of uniform flow is the starting point for describing resistance relations for all open-channel flows. If the deviations from strict uniform flow are not too great, the flow is quasi uniform, and the basic features of uniform flow will be assumed to apply.

6.2.2.1 Uniform Flow as an Asymptotic Condition

Although figure 6.2 depicts a long channel segment as having uniform flow, in fact uniform flow is approached asymptotically. As stated by Chow (1959, p. 91), "Theoretically speaking, the varied depth at each end approaches the uniform depth in the middle asymptotically and gradually. For practical purposes, however, the depth may be considered constant (and the flow uniform) if the variation in depth is within a certain margin, say, 1%, of the average uniform-flow depth." Thus, the shaded area in figure 6.2 is the portion of the flow that is within this 1% limit.

6.2.2.2 Water-Surface Stability

Under some conditions, wavelike fluctuations of the water surface prevent the attainment of truly uniform flow. As we will discuss more fully in chapter 11, a gravity wave in shallow water travels at a speed relative to the water, or **celerity**, C_{gw}, that is determined by the depth, Y:

$$C_{gw} = (g \cdot Y)^{1/2}, \tag{6.4}$$

where g is gravitational acceleration. ("Shallow" in this context means that the wavelength of the wave is much greater than the depth.) Note from figure 6.3 that this celerity is of the same order as typical river velocities. The **Froude number**, Fr, defined as

$$Fr \equiv \frac{U}{C_{gw}} = \frac{U}{(g \cdot Y)^{1/2}}, \tag{6.5}$$

is the ratio of flow velocity to wave celerity and defines the **flow regime**:[3]

> When $Fr = 1$, the flow regime is **critical**; when $Fr < 1$ it is **subcritical**, and when $Fr > 1$ it is **supercritical**.

Figure 6.4 shows the combinations of velocity and depth that define flows in the subcritical and supercritical regimes. Most natural river flows are subcritical

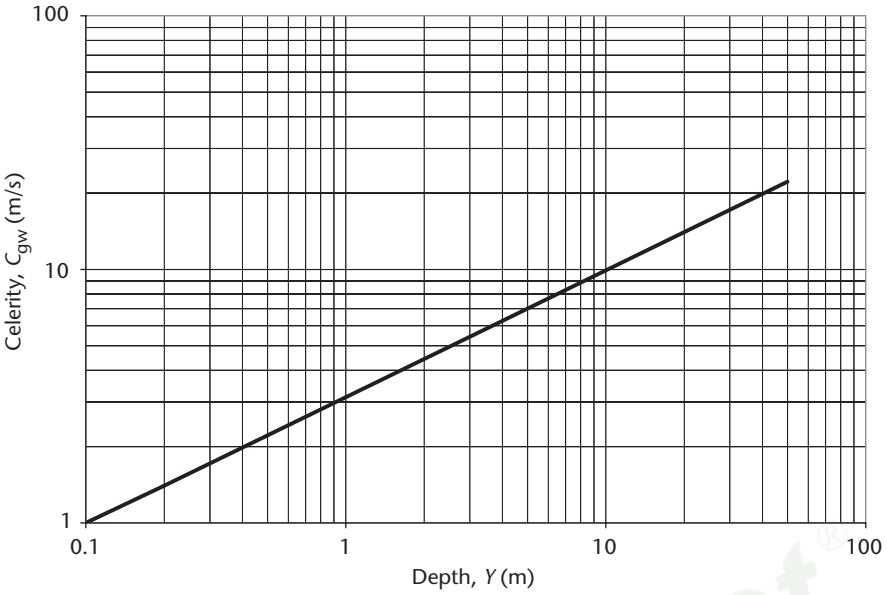

Figure 6.3 Celerity of shallow-water gravity waves, C_{gw}, as a function of flow depth, Y (equation 6.4). Note that C_{gw} is of the same order of magnitude as typical river velocities.

(Grant 1997), but when the slope is very steep and/or the channel material is very smooth (as in some bedrock channels and streams on glaciers, and at local steepenings in mountain streams), the Froude number may approach or exceed 1. When Fr approaches 1, waves begin to appear in the free surface, and strictly uniform flow is not possible. In channels with rigid boundaries, the amplitude of these waves increases approximately linearly with Fr (figure 6.5). When Fr approaches 2 (Koloseus and Davidian 1966), the flow will spontaneously form **roll waves**—the waves you often see on a steep roadway or driveway during a rainstorm (figure 6.6). However, this situation is unusual in natural channels. In channels with erodible boundaries (sand and gravel), wavelike bedforms called dunes or antidunes begin to form when Fr approaches 1. The water surface also becomes wavy, either out of phase (dunes) or in phase (antidunes) with the bedforms; these are discussed further in section 6.6.4 and in sections 10.2.1.5 and 12.5.4.

In situations where surface instabilities occur, it may be acceptable to relax the definition of "uniform" by averaging dU/dX and dY/dX over distances greater than the wavelength of the surface waves.

6.2.2.3 Secondary Currents

The concept of uniform flow as described in section 6.2.1 implicitly assumes that flow is the downstream direction only, and this assumption underlies most of the analyses in this text. However, as we saw in section 5.4.2, even in straight rectangular

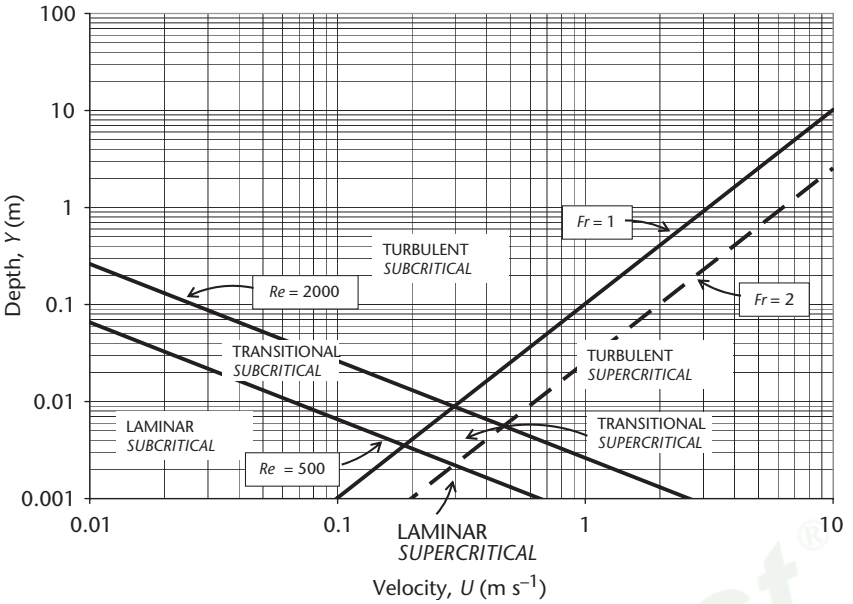

Figure 6.4 Flow states and flow regimes as a function of average velocity, U, and depth Y. The great majority of river flows are in the turbulent state ($Re > 2000$) and subcritical regime ($Fr < 1$). When the Froude number Fr (equation 6.5) approaches 1, the water surface becomes wavy, and strictly uniform flow cannot occur. When Fr approaches 2, pronounced waves are present. Note that some authors (e.g., Chow 1959) use the term "regime" to apply to one of the four fields shown on this diagram rather than to the subcritical/supercritical condition.

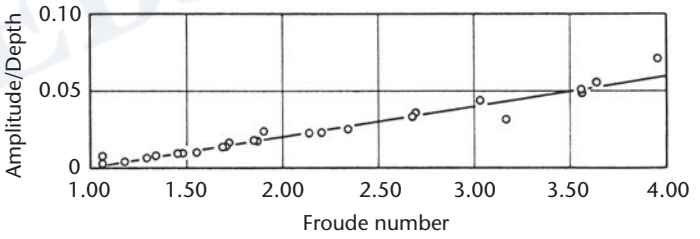

Figure 6.5 Ratio of wave amplitude to mean depth as a function of Froude number as observed in flume experiments by Tracy and Lester (1961, their figure 6).

channels spiral circulations are often present, making the velocity distribution three-dimensional and suppressing the level of maximum velocity below the surface. These secondary or helicoidal currents spiral downstream with velocities on the order of 5% of the downstream velocity and differ in direction by only a few degrees from the downstream direction (Bridge 2003). Thus, their effect on the assumptions of uniform flow is generally small.

Figure 6.6 Roll waves on a steep driveway during a rainstorm. These waves form when the Froude number approaches 2. Photo by the author.

6.3 Basic Equation of Uniform Flow: The Chézy Equation

In this section, we derive the basic equation for strictly uniform flow. This equation forms the basis for understanding fundamental resistance relations and other important aspects of flows in channel reaches.

Because there is no acceleration in a uniform flow, Newton's second law states that there are no net forces acting on the fluid and that

$$F_D = F_R, \tag{6.6}$$

where F_D represents the net forces tending to cause motion, and F_R represents the net forces tending to resist motion. The French engineer Antoine Chézy (1718–1798) was the first to develop a relation between flow velocity and channel characteristics from the fundamental force relation of equation 6.6.[4] Referring to the idealized rectangular channel reach of figure 6.7, Chézy expressed the downslope component of the gravitational force acting on the water in a channel reach, F_D, as

$$F_D = \gamma \cdot W \cdot Y \cdot X \cdot \sin\theta = \gamma \cdot A \cdot X \cdot \sin\theta, \tag{6.7}$$

where γ is the weight density of water, A is the cross-sectional area of the flow, and θ denotes the slope of the water surface and the channel, which are equal in uniform flow.

Chézy noted that the resistance forces are due to a boundary shear stress τ_0 [F L^{-2}] caused by boundary friction. This is the same quantity defined in equation 5.7, but

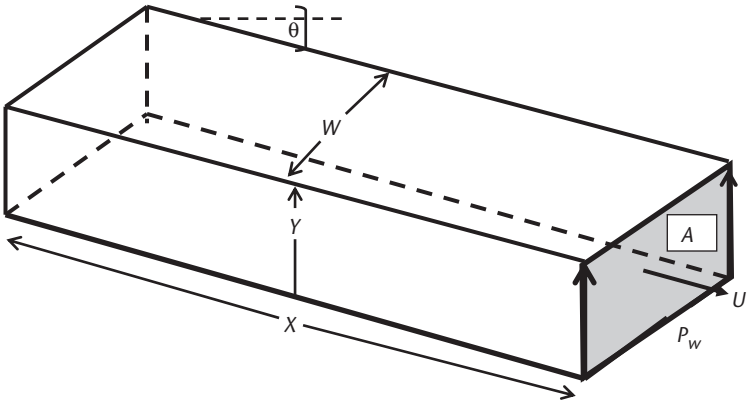

Figure 6.7 Definitions of terms for development of the Chézy relation (equation 6.15). The idealized channel reach has a rectangular cross-section of slope θ, width W, and depth Y. A is the wetted cross-sectional area (shaded), P_w is the wetted perimeter, and U is the reach-averaged velocity.

now applies to the entire cross section, not just the local channel bed. Chézy further reasoned that this stress is proportional to the square of the average velocity:

$$\tau_0 = K_T \cdot \rho \cdot U^2, \tag{6.8}$$

where K_T is a dimensionless proportionality factor. This expression is dimensionally correct and is physically justified by the model of turbulence developed in section 3.3.4, which shows that shear stress is proportional to the turbulent velocity fluctuations (equation 3.32; see also equation 5.27b) and that these fluctuations are proportional to the average velocity.[5]

This boundary shear stress acts over the area of the channel that is in contact with the water, A_B (the frictional resistance at the air-water interface is negligible), which in the rectangular channel shown in figure 6.7 is given by

$$A_B = (2Y + W) \cdot X = P_w \cdot X, \tag{6.9}$$

where P_w is the **wetted perimeter** of the flow. Thus,

$$F_R = \tau_0 \cdot A_B = K_T \cdot \rho \cdot U^2 \cdot P_w \cdot X, \tag{6.10}$$

where τ_0 designates the shear stress acting over the entire flow boundary.

Combining equations 6.6, 6.7, and 6.10 gives

$$\gamma \cdot A \cdot X \cdot \sin\theta = K_T \cdot \rho \cdot U^2 \cdot P_w \cdot X, \tag{6.11}$$

which (noting that $\gamma/\rho = g$) can be solved for U to give

$$U = \left(\frac{g}{K_T}\right)^{1/2} \cdot \left(\frac{A}{P_w}\right)^{1/2} \cdot (\sin\theta)^{1/2} \tag{6.12}$$

The ratio of cross-sectional area to wetted perimeter is called the **hydraulic radius**, R:

$$R \equiv \frac{A}{P_w}. \tag{6.13}$$

Incorporating equation 6.13 and defining

$$S \equiv \sin\theta, \tag{6.14}$$

We can write the Chézy equation as

$$U = \left(\frac{1}{K_T}\right)^{1/2} \cdot (g \cdot R \cdot S)^{1/2}. \tag{6.15a}$$

For "wide" channels we can approximate the hydraulic radius by the average depth. Thus, we can usually write the Chézy equation as

$$U = \left(\frac{1}{K_T}\right)^{1/2} \cdot (g \cdot Y \cdot S)^{1/2}. \tag{6.15b}$$

In engineering contexts, the Chézy equation is usually written as described in box 6.1.

The Chézy equation is the basic uniform-flow equation and is the basis for describing the relations among the cross-section or reach-averaged values of the fundamental hydraulic variables velocity, depth, slope, and channel characteristics. It provides a partial answer to the central question posed at the beginning of the chapter, as we have found that

> The average velocity of a uniform open-channel flow is proportional to the square root of the product of hydraulic radius (R) and the downslope component of gravitational acceleration ($g \cdot S$).

Also note that the Chézy equation was developed from force-balance considerations and is a macroscopic version of the general conductance relation (equation 4.54, section 4.7). The Chézy equation was derived by considering the water in the channel as a "block" interacting with the channel boundary; we did not consider phenomena within the "block" except to justify the relation between τ_0 and the square of the velocity (equation 6.8).

A more complete answer to the central question posed at the beginning of this chapter requires some way of determining the value of K_T. This quantity is the proportionality between the shear stress due to the boundary and the square of the velocity; thus, presumably it depends in some way on the nature of the boundary. Most of the rest of this chapter explores the relation between this proportionality and the nature of the boundary. We will see that the velocity profiles derived in chapter 5 along with experimental observations provide much of the basis for formulating this relation. But before proceeding to that exploration, we use the Chézy derivation to formulate the working definition of resistance.

6.4 Definition of Reach Resistance

By comparison with equation 5.24, the quantity $(g \cdot R \cdot S)^{1/2}$ can be considered to be the **reach-averaged shear velocity**, so henceforth

$$u_* \equiv (g \cdot R \cdot S)^{1/2}. \tag{6.16a}$$

Again, we have seen that we can usually approximate this definition as

$$u_* = (g \cdot Y \cdot S_0)^{1/2}. \tag{6.16b}$$

BOX 6.1 Chézy's *C*

In engineering texts, the Chézy equation is usually written as

$$U = C \cdot (R \cdot S)^{1/2}, \tag{6B1.1}$$

where C expresses the reach conductance and is known as "Chézy's C." Note from equation 6.15a that

$$C \equiv \left(\frac{g}{K_T} \right)^{1/2}, \tag{6B1.2}$$

and thus has dimensions $[L^{1/2}\ T^{-1}]$.

In engineering practice, however, C is treated as a dimensionless quantity so that it has the same numerical value in all unit systems. This can be a dangerous practice: equation 6B1.1 is in fact correct only if the British (ft-s) unit system is used. If C is to have the same numerical value in all unit systems, the Chézy equation must be written as

$$U = u_C \cdot C \cdot (R \cdot S)^{1/2}, \tag{6B1.3}$$

where u_C is a unit-adjustment factor that takes the following values:

Unit system	$\mathbf{u_C}$
Système Internationale	0.552
British	1.00
Centimeter-gram-second	5.52

No systematic method for estimating Chézy's C from channel characteristics has been published (Yen 2002). The following statistics from a database of 931 flows in New Zealand and the United States collated by the author give a sense of the range of C values in natural channels:

Statistic	**C value**
Mean	32.5
Median	29.3
Standard deviation	17.7
Maximum	86.6
Minimum	2.1

Using this definition, we define **reach resistance**, Ω, as the ratio of reach-averaged shear velocity to reach-averaged velocity:

$$\Omega \equiv \frac{u_*}{U}. \tag{6.17}$$

This definition simply provides us with a notation that will prove to be more convenient than using K_T: the relation between them is obviously

$$\Omega = K_T^{1/2}. \tag{6.18}$$

Box 6.2 defines the **Darcy-Weisbach friction factor**, a dimensionless resistance factor that is commonly used as an alternative to K_T and Ω.

Note that using equation 6.17, we can rewrite the Chézy equation as

$$U = \Omega^{-1} \cdot u_*. \tag{6.19}$$

BOX 6.2 The Darcy-Weisbach Friction Factor

In 1845 Julius Weisbach (1806–1871) published the results of pioneering experiments to determine frictional resistance in pipe flow (Rouse and Ince 1963) and formulated a dimensionless factor, f_{DW}, that expresses this resistance:

$$f_{DW} \equiv 2 \cdot \left(\frac{h_e}{X}\right) \cdot \left(\frac{D \cdot g}{U^2}\right), \tag{6B2.1}$$

where h_e (L) is the loss in mechanical energy per unit weight of water, or head (see equation 4.45) in distance X, D is the pipe diameter, U is the average flow velocity, and g is gravitational acceleration. In 1857, the same Henry Darcy (1803–1858) whose experiments led to Darcy's law, the central formula of groundwater hydraulics, published the results of similar pipe experiments, and f_{DW} is known as the **Darcy-Weisbach friction factor**.

The pipe diameter D equals four times the hydraulic radius, R, so

$$f_{DW} \equiv 8 \cdot \left(\frac{h_e}{X}\right) \cdot \left(\frac{R \cdot g}{U^2}\right). \tag{6B2.2}$$

The quantity h_e/X in pipe flow is physically identical to the channel and water-surface slope, $S \equiv \sin\theta$, in uniform open-channel flow, so the friction factor for open-channel flow is

$$f_{DW} \equiv 8 \cdot \frac{g \cdot R \cdot S}{U^2}. \tag{6B2.3a}$$

From the definition of shear velocity, u_* (equation 6.16a), 6B2.3a can also be written as

$$f_{DW} = 8 \cdot \frac{u_*^2}{U^2}, \tag{6B2.3b}$$

and from the definition of Ω (equation 6.17), we see that

$$f_{DW} = 8 \cdot \Omega^2; \tag{6B2.4a}$$

$$\Omega = \left(\frac{f_{DW}}{8}\right)^{1/2} = 0.354 \cdot f_{DW}^{1/2}. \tag{6B2.4b}$$

The Darcy-Weisbach friction factor is commonly used to express resistance in open channels as well as pipes. However, the Ω notation is used herein because it is simpler: It does not include the 8 multiplier and is written in terms of u_* and U rather than the squares of those quantities.

The inverse of a resistance is a conductance, so we can define Ω^{-1} as the **reach conductance**, and we can use the two concepts interchangeably. The central problem of open-channel flow can now be stated as, "What factors determine the value of Ω?"

6.5 Factors Affecting Reach Resistance in Uniform Flow

In section 4.8.2.2, we used dimensional analysis to derive equation 4.63:

$$U = f_\Omega\left(\frac{Y}{y_r}, \frac{Y}{W}, Re\right)\cdot(g\cdot Y\cdot S)^{1/2} = f_\Omega\left(\frac{Y}{y_r}, \frac{Y}{W}, Re\right)\cdot u_*, \tag{6.20}$$

where Re is the flow Reynolds number. Thus, we see that the Chézy equation is identical in form to the open-channel flow relation developed from dimensional analysis. And, comparing 6.19 and 6.20, we see that the dimensional analysis provided some clues to the factors affecting resistance/conductance:

$$\Omega = f_\Omega\left(\frac{Y}{y_r}, \frac{Y}{W}, Re\right), \tag{6.21}$$

where f_Ω denotes the resistance/conductance function. Thus, we have reason to believe that, in uniform turbulent flow, resistance depends on the **relative smoothness** Y/y_r (or its inverse, **relative roughness** y_r/Y),[6] the depth/width ratio Y/W (or W/Y), and the Reynolds number, Re. However, as we saw in section 2.4.2, most natural channels have small Y/W values, so the effects of Y/W should usually be minor; thus, we focus here on the effects of relative roughness and Reynolds number.

The nature of f_Ω has been explored experimentally in pipes and wide open channels and can be summarized as in figure 6.8. Here, Ω (y-axis) is shown as a function of Re (x-axis) and Y/y_r (separate curves at high Re) for wide open channels with rigid impervious boundaries. Graphs relating resistance to Re and Y/y_r are called **Moody diagrams** because they were first presented, for flow in pipes, by Moody (1944). The original Moody diagrams were based in part on experimental data of Johann Nikuradse (1894–1979), who measured resistance in pipes lined with sand particles of various diameters. These relations have been modified to apply to wide open channels (Brownlie 1981a; Chang 1988; Yen 2002).

Figure 6.8 reveals important aspects of the resistance relation for uniform flow. First, note that, overall, Ω tends to decrease with Re and that the $\Omega - Re$ relation f_Ω differs in different ranges of Re. For laminar flow and hydraulically smooth turbulent flow, Ω depends only on Reynolds number:

Laminar flow ($Re < 500$):

$$\Omega = \left(\frac{3}{Re}\right)^{1/2} = \frac{1.73}{Re^{1/2}}. \tag{6.22}$$

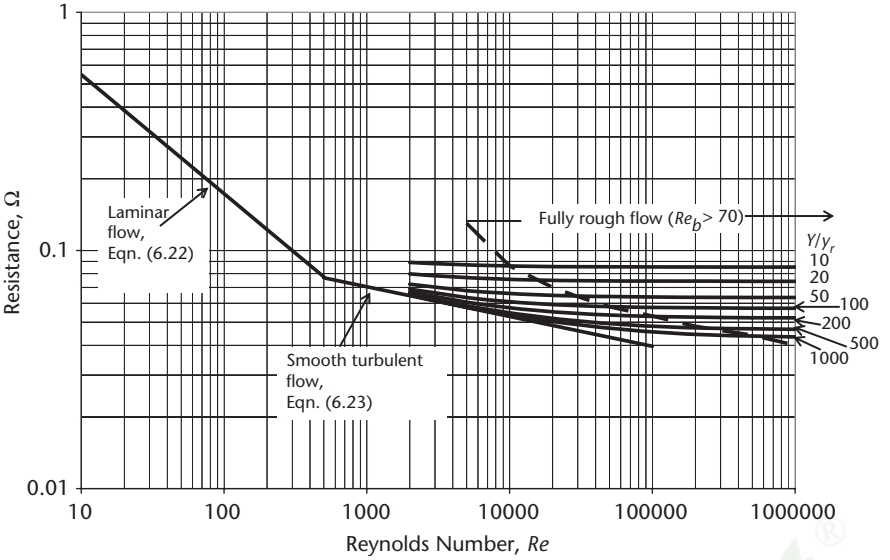

Figure 6.8 The Moody diagram: Relation between resistance, Ω; Reynolds number, Re; and relative smoothness, Y/y_r, for laminar, smooth turbulent, and rough turbulent flows in wide open channels. Y/y_r affects resistance only for rough turbulent flows ($Re > 2000$ and $Re_b > 5$). The effect of Re on resistance in rough turbulent flows decreases with Re; resistance becomes independent of Re for "fully rough" flows ($Re_b > 70$).

Smooth turbulent flow ($Re > 500$; $Re_b < 5$):

$$\Omega = \frac{0.167}{Re^{1/8}}. \tag{6.23}$$

For turbulent flow in hydraulically rough channels ($Re_b > 5$), the relation depends on both Re and Y/y_r and can be approximated by a semiempirical function proposed by Yen (2002):

$$\Omega = 0.400 \cdot \left[-\ln\left(\frac{y_r}{11 \cdot Y} + \frac{1.95}{Re^{0.9}} \right) \right]^{-1} \tag{6.24}$$

Note that at very high values of Re, the second term in 6.24 becomes very small and resistance depends only on Y/y_r (i.e., the curves become horizontal); this is the region of **fully rough flow**, $Re_b > 70$. The transition to fully rough flow occurs at lower Re values as the boundary gets relatively rougher (i.e., as Y/y_r decreases). Figure 6.9 shows the relation between Ω and Y/y_r given by 6.24 for fully rough flow, that is, where

$$\Omega_* = 0.400 \cdot \left[-\ln\left(\frac{y_r}{11 \cdot Y} \right) \right]^{-1} = 0.400 \cdot \left[\ln\left(\frac{11 \cdot Y}{y_r} \right) \right]^{-1}. \tag{6.25}$$

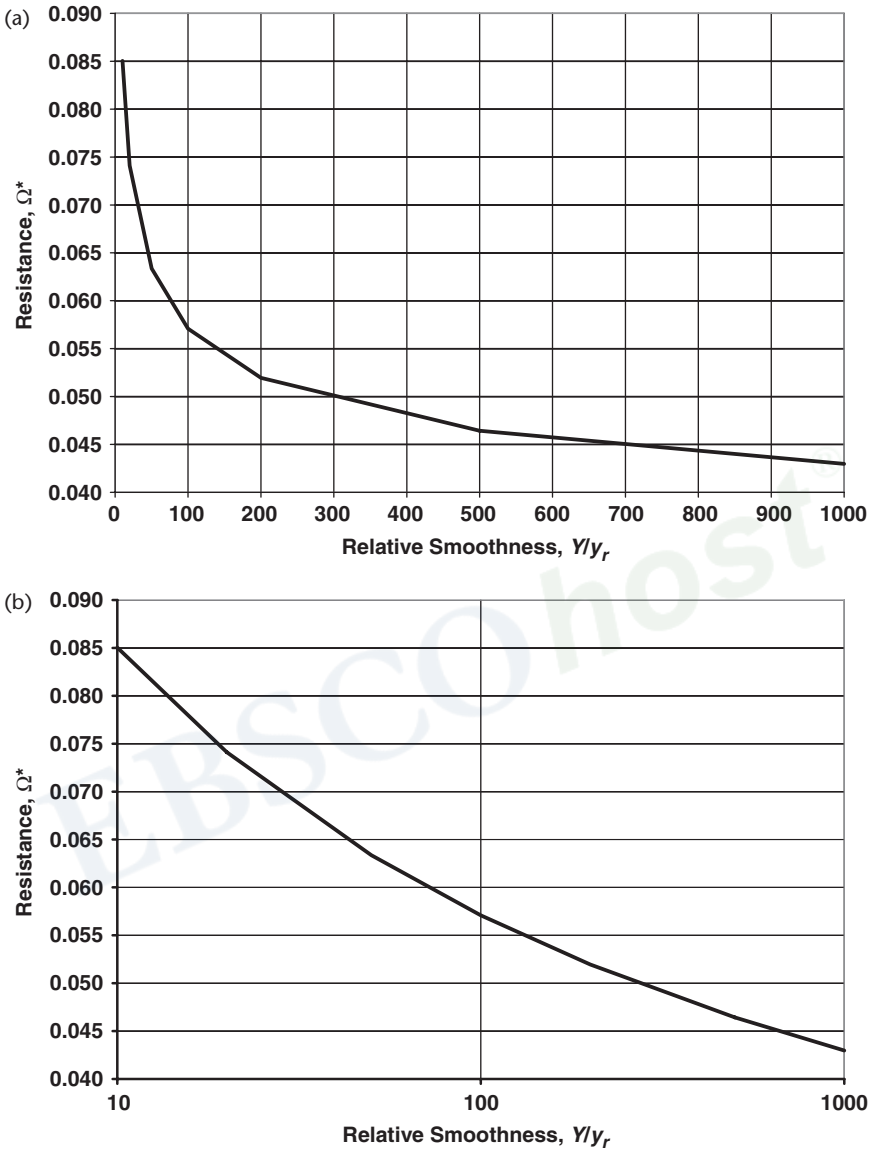

Figure 6.9 Baseline resistance, Ω_*, as a function of relative smoothness, Y/y_r, for fully rough turbulent flow in wide channels as given by equation 6.25. This is identical to the relation given by the integrated P-vK velocity profile (equation 6.26). (a) Arithmetic plot; (b) semilogarithmic plot.

In the reminder of this chapter, we designate the resistance given by 6.25 as Ω_* and use it to represent a baseline resistance value that applies to rough turbulent flow in wide channels.

In general, natural channels will have a resistance greater than Ω_* due to the complex effects of many factors that affect resistance in addition to Y/y_r and Re. These additional factors are explored in section 6.6.

For fully rough flow and very large values of Re, equation 6.25 can be inverted and written as

$$U = 2.50 \cdot u_* \cdot \ln\left(\frac{11 \cdot Y}{y_r}\right), \tag{6.26}$$

a form that looks similar to the vertically integrated P-vK velocity profile (equation 5.34a–d). In fact, if we combine equations 5.39–5.41 and recall from equation 5.32b that $y_0 = y_r/30$ for rough flow, the integrated P-vK law is identical to equation 6.26. This should not be surprising, given that the integrated P-vK profile gives the average velocity for a wide open channel. Equation 6.26 is often called the **Keulegan equation** (Keulegan 1938); we will refer to it as the **Chézy-Keulegan** or **C-K equation**.

We can summarize resistance relations for uniform turbulent flows in wide open channels with rigid impervious boundaries as follows:

- Although width/depth ratio potentially affects reach resistance, most natural flows have width/depth values so high that the effect is negligible.
- In smooth flows, resistance decreases as the Reynolds number increases.
- In rough flows with a given relative roughness, resistance decreases as the Reynolds number increases until the flow becomes fully rough, beyond which it ceases to depend on the Reynolds number.
- In rough flows at a given Reynolds number, resistance increases with relative roughness.
- In wide fully rough flows, resistance depends only on relative roughness and the relation between resistance and relative roughness is given by the integrated P-vK profile (C-K equation).

6.6 Factors Affecting Reach Resistance in Natural Channels

The analysis leading to equation 6.21 indicates that resistance in uniform flows in prismatic channels is a function of the relative smoothness, Y/y_r; the Reynolds number, Re; and the depth/width ratio, Y/W. Because flow resistance is determined by any feature that produces changes in the magnitude or direction of the velocity vectors, we can expect that resistance in natural channels is also affected by additional factors. We will use the quantity $(\Omega - \Omega_*)/\Omega_*$ to express the dimensionless "excess" resistance in a reach, that is, the difference between actual resistance Ω and the resistance computed via equation 6.25. Figure 6.10 shows this quantity plotted against Y/W for a database of 664 flows in natural channels. Although for many of these flows actual resistance is close to that given by 6.25 [i.e., $(\Omega - \Omega_*)/\Omega_* = 0$], a great majority (86%) have higher resistance, and some have resistances several times Ω_*. This plot

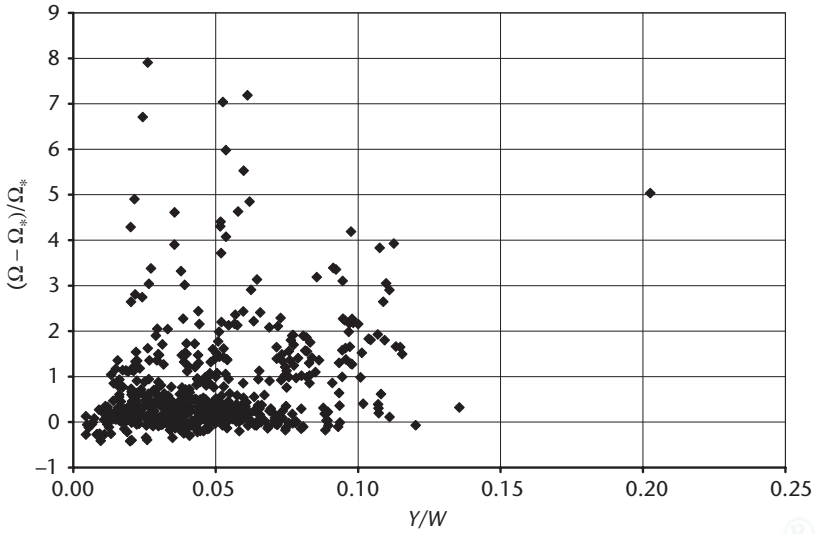

Figure 6.10 Ratio of "excess" resistance to baseline resistance computed from equation 6.25, $(\Omega - \Omega_*)/\Omega_*$, plotted against Y/W for a database of 664 flows in natural channels. Most (86%) of these flows have resistance greater than Ω_*. Clearly, the additional resistance is due to factors other than Y/W.

clearly indicates that, in general, factors other than Y/W cause "excess" resistance in natural channels.

The following subsections discuss, for each of four classes of factors that may produce this excess resistance, 1) approaches to quantifying its contribution, and 2) evidence from field and laboratory studies that gives an idea of the magnitude of the excess resistance produced. Keep in mind, however, that the variability of natural rivers makes this a very challenging area of research and that the approaches and results presented here are not completely definitive.

6.6.1 Effects of Channel Irregularities

Clearly, any irregularities in channel geometry will cause velocity vectors to deviate from direct downstream flow, producing accelerations and concomitant increases in resisting forces. Figure 6.11 shows three categories of geometrical irregularities: in cross section, in plan (map) view, and in reach-scale longitudinal profile (slope). These geometrical irregularities are usually the main sources of the excess resistance apparent in figure 6.10.

6.6.1.1 Cross-section Irregularities

Equation 6.25 gives resistance in hydraulically rough flows in wide open channels in which the depth is constant, the P-vK velocity profile applies at all locations in the

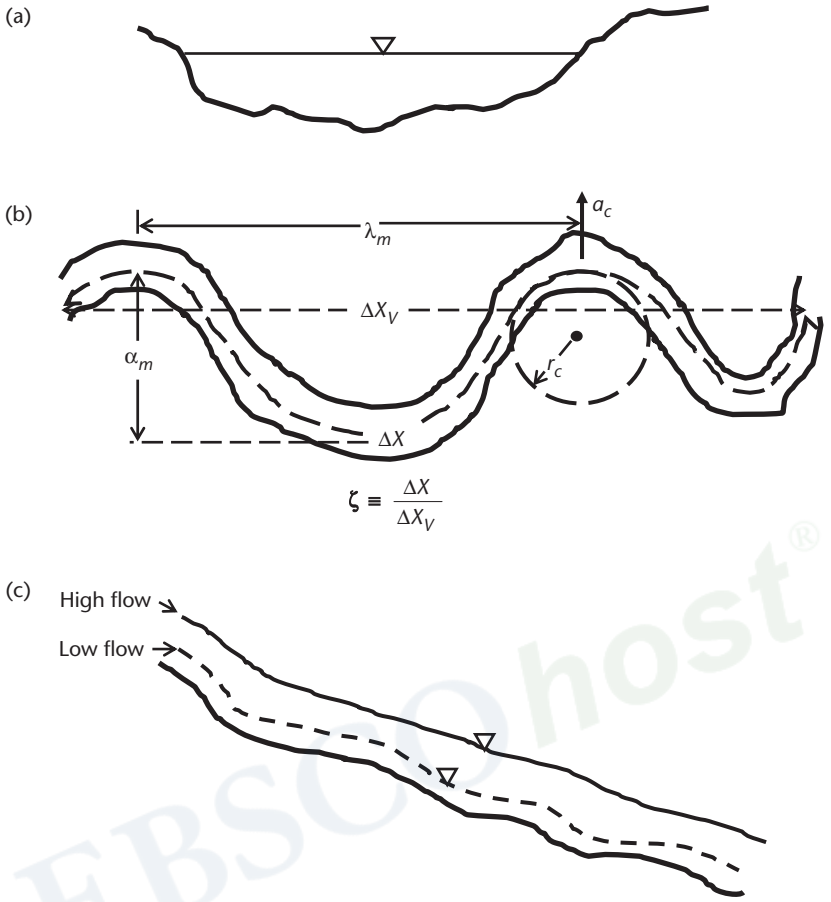

Figure 6.11 Three categories of channel irregularity that cause changes in the magnitude and/or direction of velocity vectors and hence increase flow resistance beyond that given by equation 6.25. (a) Irregularities in cross-section. (b) Irregularities in plan (map) view. ζ designates sinuosity, the streamwise distance ΔX divided by the valley distance ΔX_v; r_c is the radius of curvature of a river bend, λ_m is meander wavelength, a_m is meander amplitude, and a_c represents the centrifugal acceleration. (c) Reach-scale irregularities in longitudinal profile (channel slope); these are more pronounced at low flows and less pronounced at high flows.

cross section, and the only velocity gradients are "vertical." Under these conditions, the isovels (lines of equal velocity) are straight lines parallel to the bottom.

As shown in figure 6.12, irregularities in cross section (represented here by the sloping bank of a trapezoidal channel) cause deviations from this pattern and introduce horizontal velocity gradients that increase shear stress and produce excess resistance. These effects are also apparent in figure 5.22, which shows isovels in two natural channels, where bottom irregularities and other factors produce marked horizontal velocity gradients and significant excess resistance. The presence of obstructions also

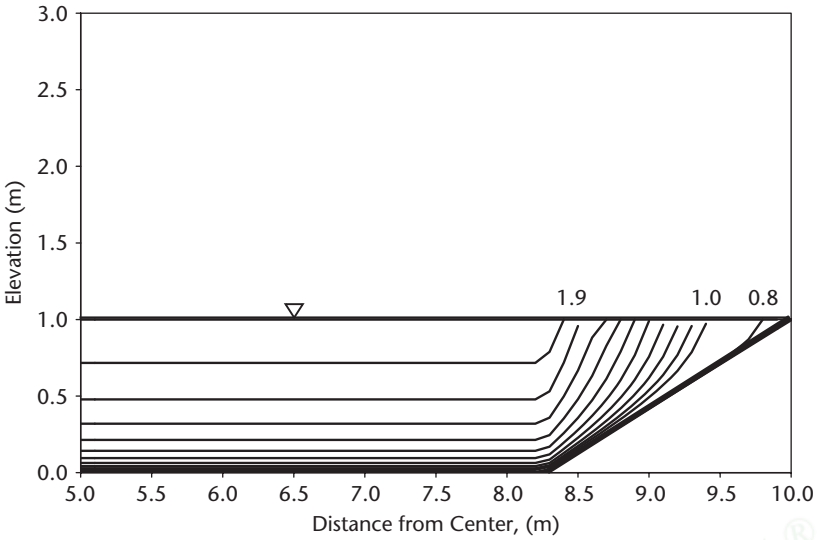

Figure 6.12 Isovels in the near-bank portion of an idealized flow in a trapezoidal channel. The P-vK vertical velocity distribution applies at all points; contours are in m/s. Cross-section irregularities, represented here by the sloping bank, induce horizontal velocity gradients that increase turbulent shear stress and therefore resistance.

induces secondary circulations and tends to suppress the maximum velocity below the surface (see figures 5.17, 5.19, and 5.20), further increasing resistance.

These effects are very difficult to quantify. However, the effects of cross-section irregularity should tend to diminish as depth increases in a particular reach, so at least to some extent these effects are accounted for by the inclusion of the relative smoothness Y/y_r in equation 6.25. Apparently, there been no systematic studies attempting to relate resistance to some measure of the variation of depth in a reach or cross section (e.g., the standard deviation of depth).

Bathurst (1993) reviewed resistance equations for natural streams in which gravel and boulders are a major source of cross-section irregularity. For approximately uniform flow in gravel-bed streams, he found that resistance could be estimated with ±30% error as

$$\Omega = 0.400 \cdot \left[-\ln\left(\frac{d_{84}}{3.60 \cdot R} \right) \right]^{-1}, \tag{6.27}$$

for reaches in which 39 mm $\leq d_{84} \leq$ 250 mm and $0.7 \leq R/d_{84} \leq 17$. For boulder-bed streams, Bathurst (1993) suggested the following equation, which is based on data from flume and field studies:

$$\Omega = 0.410 \cdot \left[-\ln\left(\frac{d_{84}}{5.15 \cdot R} \right) \right]^{-1}, \tag{6.28}$$

for reaches in which $0.004 \leq S \leq 0.04$ and $R/d_{84} \leq 10$. Note that the form of equations 6.27 and 6.28 is identical to that of equation 6.25, assuming $y_r = d_{84}$.

Figure 6.13 shows that excess resistance for gravel and boulder-bed streams given by equations 6.27 and 6.28 is typically in the range of 20% to well more than 50%. However, it seems surprising that resistance in gravel-bed streams is larger than in boulder-bed streams, and this result may reflect the very imperfect state of knowledge about resistance in natural streams, as Bathurst (1993) emphasizes. In some recent studies, Smart et al. (2002) developed similar relations for use in the relative-roughness range $5 \leq R/d_{84} \leq 20$, and Bathurst (2002) recommended computing resistance as a function of R/d_{84} via the formulas shown in table 6.1 as *minimum* values for resistance in mountain rivers with $R/d_{84} < 11$ and $0.002 \leq S_0 \leq 0.04$.

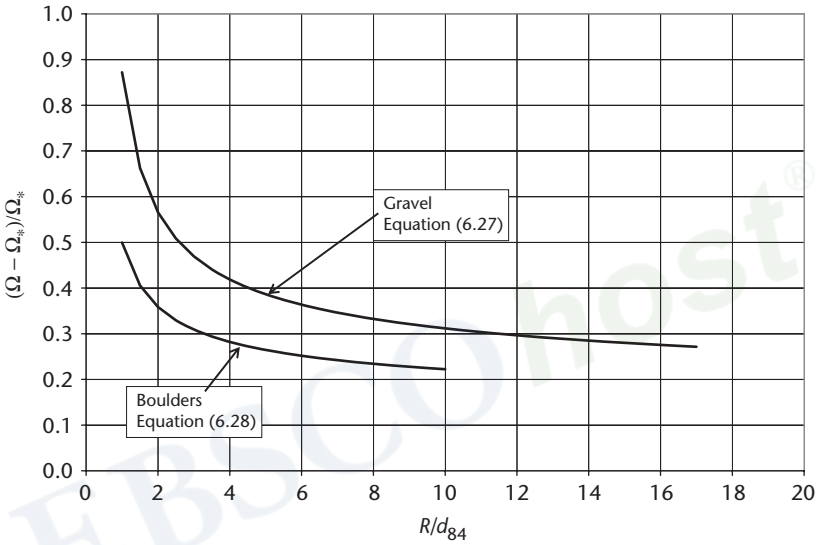

Figure 6.13 Ratio of excess resistance to baseline resistance for gravel and boulder-bed streams according to Bathurst (1993) (equations 6.27 and 6.28). Values are typically in the range of 20% to well more than 50%.

Table 6.1 Minimum values of resistance recommended by Bathurst (2002) for mountain rivers with $R/d_{84} < 11$ and $0.002 \leq S_0 \leq 0.04$.[a]

Slope range	Resistance (Ω)
$0.002 \leq S_0 \leq 0.008$	$3.84 \cdot \left(\frac{Y}{d_{84}}\right)^{0.547}$
$0.008 \leq S_0 \leq 0.04$	$3.10 \cdot \left(\frac{Y}{d_{84}}\right)^{0.93}$

[a]These values apply to situations in which resistance is primarily due to bed roughness; variations in planform, longitudinal profile, vegetation, and so forth, increase Ω beyond values given here.

6.6.1.2 Plan-View Irregularities

As we saw in section 2.2, few natural river reaches are straight, and there are several ways in which plan-view irregularities can be characterized. The overall degree of deviation from a straight-line path is the sinuosity, ζ, defined as the ratio of streamwise distance to straight-line distance (figure 6.11b). The local deviation from a straight-line path can be quantified as the radius of curvature, r_c (figure 6.11b).

From elementary physics, we know that motion with velocity U in a curved path with a radius of curvature r_c produces a **centrifugal acceleration** a_c where

$$a_c = \frac{U^2}{r_c}. \tag{6.29}$$

This acceleration multiplied by the mass of water flowing produces an apparent force, and because this force is directed at right angles to the downstream direction, it adds to the overall flow resistance.

Because velocity is highest near the surface, water near the surface accelerates more than that near the bottom; this produces secondary circulation in bends, with surface water flowing toward the outside of the bend and bottom water flowing in the opposite direction (see figure 5.21a). Thus, curvature enhances the secondary currents, increasing the resistance beyond that due to the curved flow path alone (Chang 1984).

The magnitude of the resistance due to curvature computed from a set of laboratory experiments (see box 6.3) is shown in figure 6.14. The data indicate that resistance can be increased by a factor of 2 or more when U^2/r_c exceeds 0.8 m/s^2 or sinuosity exceeds 1.04; as noted by Leopold (1994, p. 64), these experiments showed that "the frictional loss due to channel curvature is much larger than previously supposed." Sinuosities of typical meandering streams range from 1.1 to about 3.

6.6.1.3 Longitudinal-Profile Irregularities

At the reach scale, the longitudinal profiles of many streams have alternating steeper and flatter sections. In meandering streams (see section 2.2.3), the spacing of pools usually corresponds closely to the spacing of meander bends, so that pools tend to occur at spacings of about five times the bankfull width (equation 2.14). Steep mountain streams (see section 2.2.5, table 2.4) are characterized by relatively deep pools separated by steep rapids or cascades (step/pool reaches). On gentler slopes, the pools are shallower and separated by rapids (pool/riffle reaches).

The Chézy equation (equation 6.15) shows that velocity is proportional to the square root of slope. Thus, variations in slope produce accelerations and decelerations, vertical deflections of velocity vectors, and changes in depth along a river's course. Where longitudinal slope alterations are marked, they are typically a major component of overall resistance (Bathurst 1993). However, the effect in a given reach is dependent on discharge: At high flows, the water surface smoothes out and is less affected by alterations in the channel slope, whereas at low flows,

BOX 6.3 Flume Experiments on Resistance in Sinuous Channels

Leopold et al. (1960) conducted a series of experiments in a tiltable flume with a length of 15.9 m. Sand with a median diameter of 2 mm was placed in the flume, and a template was designed that could mold straight or curved trapezoidal channels in the sand. Once the channels were molded, they were coated with adhesive to prevent erosion. Plan-view geometries were as in table 6B3.1.

Table 6B3.1

Wavelength λ (m)	Radius of curvature r_c (m)	Sinuosity ζ
Straight	Straight	1.000
1.22	1.01	1.024
1.18	0.58	1.056
0.65	0.31	1.048
0.70	0.19	1.130

Flows were run at two depths; cross-section geometries were as in table 6B3.2.

Table 6B3.2

Maximum depth Y_m(m)	Bottom width W_b(m)	Water-surface width W (m)	Average depth Y (m)	Cross-sectional area A (m^2)	Wetted perimeter P_w (m)	Hydraulic radius R (m)
0.027	0.117	0.191	0.020	0.00418	0.209	0.020
0.041	0.117	0.224	0.027	0.00697	0.252	0.028

For each run, slope (S) and discharge (Q) could be set to obtain constant depth (uniform flow) throughout. The ranges of velocities (U), Reynolds numbers (Re) and Froude numbers (Fr) observed are listed in table 6B3.3.

Table 6B3.3

	S	Q (m^3/s)	U (m/s)	Re	Fr
Maximum	0.0118	0.00326	0.466	12100	0.970
Minimum	0.00033	0.00048	0.097	2130	0.187

The results of these experiments were used to plot figure 6.14 and gain quantitative insight on the effects of curvature on resistance.

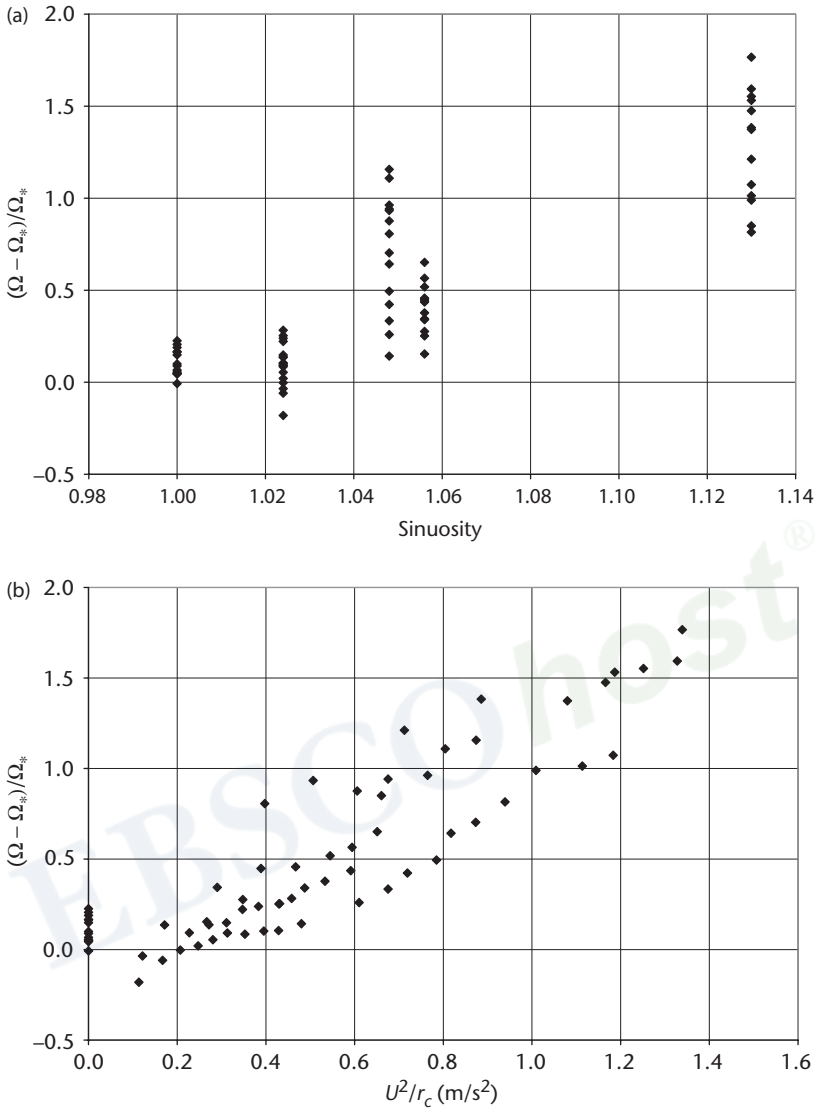

Figure 6.14 Effects of plan-view curvature on flow resistance from the experiments of Leopold et al. (1960) (see box 6.3). Excess resistance, $(\Omega - \Omega_*)/\Omega_*$, is plotted against (a) sinuosity, ζ and (b) centrifugal acceleration, $a_c = U^2/r_c$.

water-surface slope tends to parallel the local bottom slope and be more variable (figure 6.11c).

In one of the few detailed hydraulic studies of pool/fall streams, Bathurst (1993) measured resistance at three discharges in a gravel-bed river in Britain. As shown in figure 6.15, the effects of step/pool configuration are very pronounced at low discharges (low relative smoothness) and decline as discharge increases.

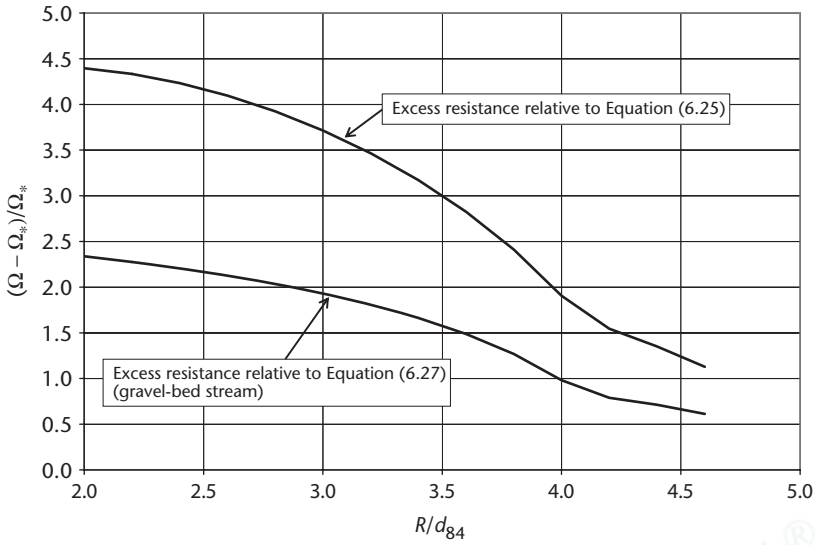

Figure 6.15 Excess resistance due to slope variations in a gravel-bed step-pool stream (River Swale, UK). The upper curve shows the excess resistance computed relative to the baseline relation (equation 6.25); the lower curve shows the excess relative to that of a uniform gravel stream (equation 6.27). The effect of the slope alterations decreases at higher discharges (higher relative smoothness). Data from Bathurst (1993).

6.6.2 Effects of Vegetation

Floodplains are commonly covered with brush or trees, and active channels can also contain living and dead plants. The effects of vegetation on resistance are complex and difficult to quantify; the major considerations are the size and shape of plants, their spacing, their heights, and their flexibility. The effects can change significantly during a particular flow event due to relative submergence and to the bending of flexible plants. Over longer time periods, the height and spacing of plants can vary seasonally and secularly due to, for example, anthropogenic increases in nutrients contained in runoff or simply to ecological processes (succession) or tree harvesting.

Kouwen and Li (1980) formulated an approach to estimating vegetative resistance that is conceptually similar to that of equations 6.27 and 6.28:

$$\Omega = k_{\text{veg}} \cdot \left[-\ln\left(\frac{y_{\text{veg}}}{K_{\text{veg}} \cdot Y} \right) \right]^{-1}, \tag{6.30}$$

where y_{veg} is the deflected vegetation height, and k_{veg} and K_{veg} are parameters. Approaches to determining values of y_{veg}, k_{veg}, and K_{veg} are given by Kouwen and Li (1980). Arcement and Schneider (1989) presented detailed field procedures

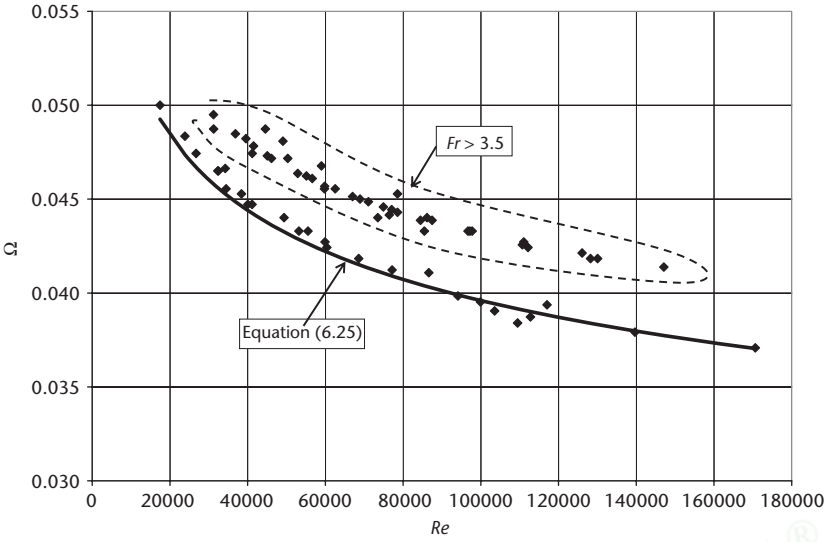

Figure 6.16 Plot of flow resistance, Ω, versus Reynolds number, *Re*, showing the effect of surface instability on flow resistance. The curve is the standard resistance relation for smooth channels given in equation 6.25; the points are resistance values measured in flume experiments of Sarma and Syala (1991). The points clustering close to the curve have $1 < Fr < 3.5$; those plotting substantially above the curve have $Fr > 3.5$.

for estimating resistance due to vegetation on floodplains. Recent analyses and experiments evaluating resistance due to vegetation are given by Wilson and Horritt (2002) and Rose et al. (2002) and summarized by Yen (2002).

6.6.3 Effects of Surface Instability

As noted in section 6.2.2.2, wavelike fluctuations begin to appear in the surfaces of open-channel flows as the Froude number *Fr* approaches 1. A few experimental studies in flumes have examined the effects of these instabilities on flow resistance.

Figure 6.16 summarizes measurements of supercritical flows in a straight, smooth, rectangular flume (Sarma and Syala 1991). It shows that for flows with $1 < Fr < 3.5$, flow resistance is essentially as predicted by the standard relation for smooth turbulent flows (equation 6.25). However, when *Fr* exceeds a threshold value of about 3.5, there is a discontinuity, and resistance jumps to a value about 10% larger than the standard value. Because Froude numbers in natural channels seldom exceed 1, Sarma and Syala's (1991) results suggest that one can usually safely ignore the effects of surface instabilities on resistance in straight channels.

However, the experiments of Leopold et al. (1960) described in box 6.3 indicate the existence of discontinuities in resistance that they attributed to surface instabilities

at channel bends and called **spill resistance**. These sudden increases in resistance occurred at Froude numbers in the range of 0.4−0.55, much lower than found by Sarma and Syala (1991) in straight smooth flumes. Thus, spill resistance may be a significant contributor to excess resistance at high flows in channel bends.

6.6.4 Effects of Sediment

Sediment transport affects flow resistance in two principal ways: 1) the effects of suspended sediment on turbulence characteristics, and 2) the effects of bedforms that accompany sediment transport on channel-bed configuration.

6.6.4.1 Effects of Sediment Load

As noted in section 5.3.1.4, there is evidence that suspended sediment suppresses turbulence and causes the value of von Kármán's constant, κ, to decrease below its clear-water value of $\kappa = 0.4$. Evidence analyzed by Einstein and Chien (1954) suggested values as low as $\kappa = 0.2$ at high sediment concentrations. Because the coefficient in equation 6.25 is κ, this suggests that resistance could be as little as 50% of its clear-water value in flows transporting sediment.

However, some researchers contend that κ remains constant and the observed resistance reduction in flows transporting sediment is due to an altered velocity distribution such that, in sediment-laden flows, velocities near the bed are reduced and those near the surface increased compared with the values given by the P-vK law (Coleman 1981; Lau 1983). Other studies have even suggested that resistance is generally increased sediment-laden flows compared with clear-water flows under identical conditions (Lyn 1991). Clearly this is a question that requires further research.

6.6.4.2 Effects of Bedforms

Observations of rivers and experiments in flumes (e.g., Simons and Richardson 1966) have revealed that in flows over sand beds, there is a typical sequence of bedforms that occurs as discharge changes. These forms are intimately related to processes of erosion that begin when the critical value of boundary shear stress, τ_0, is reached,[7] and in turn they strongly affect the velocity because of their effects on flow resistance.

The bedforms are described and illustrated in table 6.2 and figures 6.17–6.19, and figure 6.20 shows qualitatively how resistance changes through the sequence. In general, resistance increases directly with bedform height (amplitude) and inversely with bedform wavelength.

Bathurst (1993) developed an approach to accounting for these effects that involves computing the effective roughness height of the bedforms, y_{bf}, as a function of grain size, d_{84}; bedform amplitude, $\mathcal{A}_{bf}$; and bedform wavelength, λ_{bf}:

$$y_{bf} = 3 \cdot d_{84} + 1.1 \cdot \mathcal{A}_{bf} \cdot [1 - exp(-25 \cdot \mathcal{A}_{bf}/\lambda_{bf})] \tag{6.31}$$

Table 6.2 Bedforms in sand-bed streams (see figures 6.17–6.20).

	Bedform	Description	Amplitude	Wavelength	Migration velocity (mm/s)	Ω_{bf}
Lower flow regime, $Fr < 1$	Plane bed	Generally flat bed, often with irregularities due to deposition; occurs in absence of erosion.				0.05–0.06
	Ripples	Small wavelike bedforms; may be triangular to sinusoidal in longitudinal cross section. Crests are transverse to flow and may be short and irregular to long, parallel, regular ridges; typically migrate downstream at velocities much lower than stream velocity; may occur on upslope portions of dunes.	< 40 mm; mostly 10–20 mm	< 60 mm	0.1–1	0.07–0.1
	Dunes	Larger wavelike forms with crests transverse to flow, out of phase with surface waves; generally triangular in longitudinal cross section with gentle upstream slopes and steep downstream slopes. Crest lengths are approximately same magnitude as wavelength; migrate downstream at velocities much lower than stream velocity.	0.1–10 m; usually $\approx 0.1 \times Y$ to $0.3 \times Y$	0.1–100 m, usually $\approx 2 \times Y$ to $10 \times Y$	0.1–1	0.07–0.14
Upper flow regime, $Fr > 1$	Plane bed	Often occurs with heterogeneous, irregular forms; a mixture of flat areas and low-amplitude ripples and/or dunes.	< 3 mm	Irregular	10	0.05–0.06
	Antidunes	Large wavelike forms with triangular to sinusoidal longitudinal cross sections that are in phase with water-surface waves. Crest lengths approximately equal wavelength; may migrate upstream or downstream or remain stationary.	30–100 mm	$2 \cdot \pi \cdot Y$	Variable	0.05–0.06
	Chutes and pools	Large mounds of sediment that form steep chutes in which flow is supercritical, separated by pools in which flow may be subcritical or supercritical. Hydraulic jumps (see chapter 10) form at supercritical-to-subcritical transitions; migrate slowly upstream.			1–50	

After Task Force on Bed Forms in Alluvial Channels (1966) and Bridge (2003).

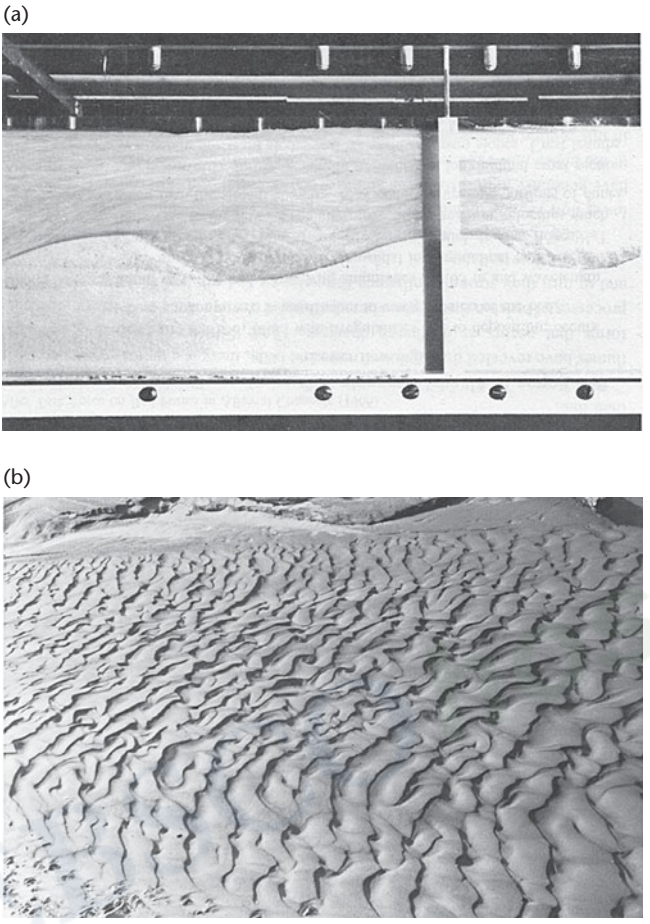

Figure 6.17 Ripples. (a) Side view of ripples in a laboratory flume. The flow is from left to right at a mean depth of 0.064 m and a mean velocity of 0.43 m/s ($Fr = 0.54$). Aluminum powder was added to the water to make the flow paths visible. Note that the water surface is unaffected by the ripples. Photograph courtesy of A. V. Jopling, University of Toronto. (b) Ripples on the bed of the Delta River in central Alaska. Flow was from left to right.

Resistance is then computed as

$$\Omega = 0.400 \cdot \left[-\ln\left(\frac{y_{bf}}{12.1 \cdot R}\right)\right]^{-1}, \tag{6.32}$$

where R is hydraulic radius ($\approx Y$ for wide channels).

In another approach, the resistance is separated into 1) that due to the bed material (the plane-bed resistance Ω_* given by equation 6.25) and 2) that due to the bedforms, Ω_{bf}:

$$\Omega = \Omega_* + \Omega_{bf}. \tag{6.33}$$

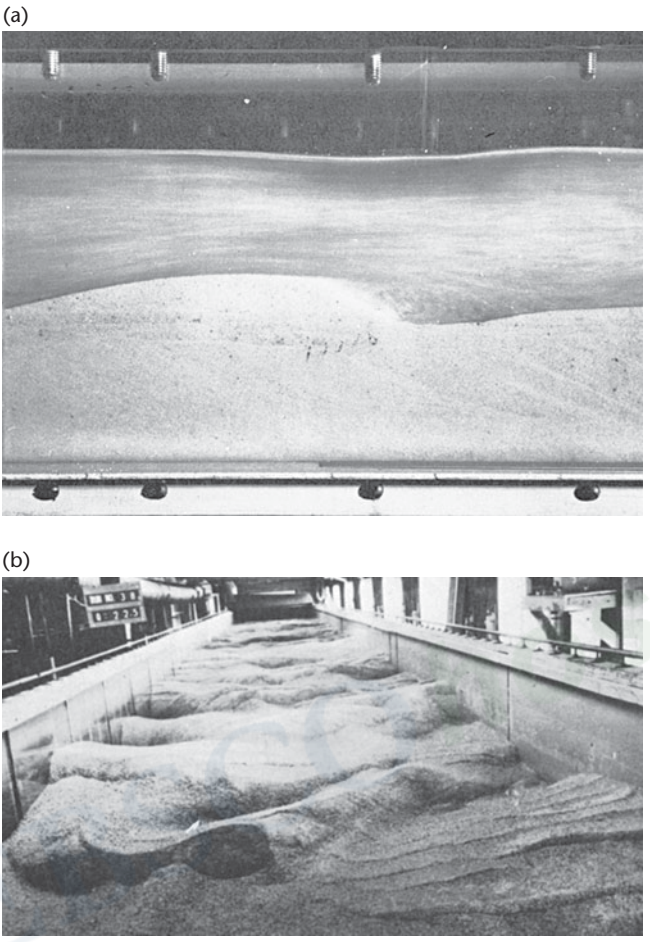

Figure 6.18 Dunes. (a) Side view of dunes in a laboratory flume. The flow is from left to right at a mean depth of 0.064 m and a mean velocity of 0.67 m/s ($Fr = 0.85$). Aluminum powder was added to the water to make the flow paths visible. Note that the water surface is out of phase with the bedforms. Photograph courtesy of A.V. Jopling, University of Toronto. (b) Dunes in a laboratory flume. Flow was toward the observer at a mean depth of 0.31 m and a mean velocity of 0.85 m/s ($Fr = 0.49$). Note ripples superimposed on some dunes. Photograph courtesy of D.B. Simons, Colorado State University.

Yen (2002) reviews several approaches to estimating Ω_{bf}; some typical values are indicated in table 6.2.

6.6.5 Effects of Ice

As noted in section 3.2.2.3, the presence of an ice cover or frazil ice can significantly increase resistance. For a uniform flow in a rectangular channel (figure 6.7), the effect

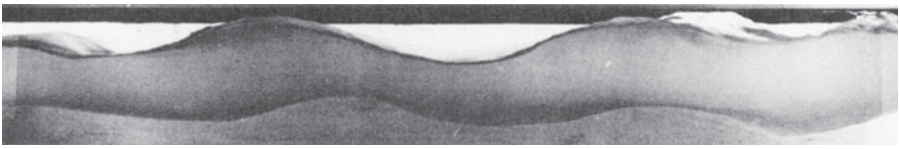

Figure 6.19 Side view of antidunes in a laboratory flume The flow is from left to right at a mean depth of 0.11 m and a mean velocity of 0.79 m/s ($Fr = 0.76$). Note that the surface waves are approximately in phase with the bedforms, which are also migrating to the right. Photograph courtesy of J. F. Kennedy, University of Iowa.

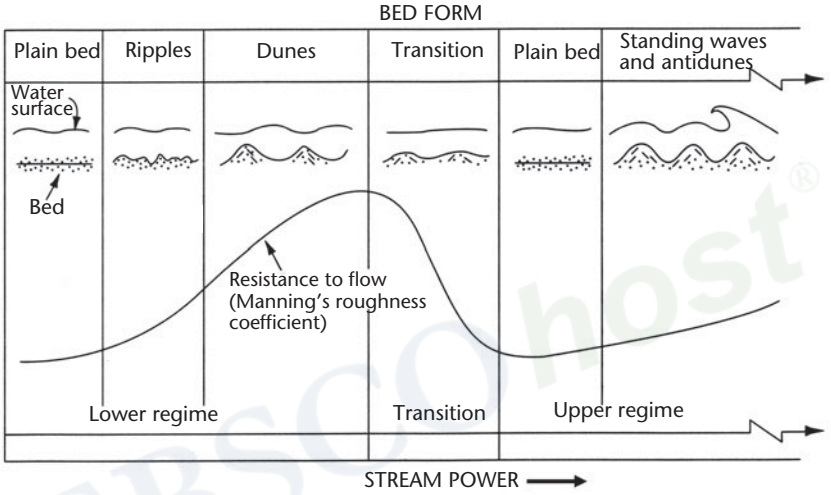

Figure 6.20 Sequence of bedforms and flow resistance in sand-bed streams. From Arcement and Schneider (1989). See table 6.2 for typical Ω values.

of an ice cover can be included in formulating the expression for the resisting forces, so that equation 6.10 becomes

$$F_R = \tau_B \cdot (2 \cdot Y + W) \cdot X + \tau_I \cdot W \cdot X, \tag{6.34}$$

where τ_B is the shear stress on the bed and τ_I is the shear stress on the ice cover. If this force balances the downstream-directed force (equation 6.7) and we assume a wide channel (i.e., $P_w = W$), the modified Chézy equation becomes

$$U = (\Omega_B^2 + \Omega_I^2)^{-1/2} \cdot u_*, \tag{6.35}$$

where Ω_B and Ω_I are the resistances due to the bed and the ice cover, respectively.

One would expect Ω_I to vary widely in natural streams due to 1) variations in the degree of ice cover, 2) development of ripplelike and dunelike bedforms on the underside of the ice cover (Ashton and Kennedy 1972), 3) development of partial or complete ice jamming, and 4) the concentration of frazil ice in the flow. An analysis of ice resistance on the St. Lawrence River by Tsang (1982) indicates that Ω_I is on

the order of $0.7-1.5$ times Ω_B, and data presented by Chow (1959) suggest values in the range from $\Omega_I = 0.03$ for smooth ice without ice blocks to $\Omega_I = 0.085$ for rough ice with ice blocks. White (1999) and Brunner (2001b) summarized resistance due to ice given by several studies; these cover a very wide range of values.

6.7 Field Computation of Reach Resistance

Validation of methods of determining reach resistance requires comparison with actual resistance values. The method developed here to compute resistance in natural, nonprismatic channels is based closely on the concepts used to derive the Chézy equation for uniform flow in prismatic channels in section 6.3.

Designating X as the distance measured along the stream course, the cross-sectional area, A, wetted perimeter, P_w, hydraulic radius, R, and water-surface slope, S_S, vary through a natural-channel reach (figure 6.21) and so are written as functions of X: $A(X)$, $P_w(X)$, $R(X)$, and $S_S(X)$ respectively. With this notation, the downstream-directed force, F_D, is

$$F_D = \gamma \cdot \int_{X_0}^{X_N} A(X) \cdot S_S(X) \cdot \mathrm{d}X, \tag{6.36}$$

where X_0 and X_N are the locations of the upstream and downstream boundaries of the reach, respectively. Note that this expression is analogous to equation 6.7, but for nonprismatic rather than prismatic channels.

Similarly, the upstream-directed resistance force, F_R in a nonprismatic channel is

$$F_R = K_T \cdot \rho \cdot U^2 \cdot \int_{X_0}^{X_N} P_w(X) \cdot \mathrm{d}X, \tag{6.37}$$

where U is the reach-average velocity. This expression is analogous to equation 6.10.

For a given discharge, Q, the reach-average velocity is

$$U = \frac{Q}{\left(\frac{1}{\Delta X}\right) \cdot \int_{X_0}^{X_N} A(X) \cdot \mathrm{d}X}. \tag{6.38}$$

where $\Delta X \equiv X_N - X_0$.

Equating F_D and F_R as in equation 6.6, substituting equations 6.36–6.38, and solving for K_T gives

$$K_T = \frac{g \cdot \int_{X_0}^{X_N} A(X) \cdot S_S(X) \cdot \mathrm{d}X \cdot \left[\int_{X_0}^{X_N} A(X) \cdot \mathrm{d}X\right]^2}{Q^2 \cdot \Delta X^2 \cdot \int_{X_0}^{X_N} P_w(X) \cdot \mathrm{d}X} = \Omega^2; \tag{6.39a}$$

$$\Omega = \frac{g^{1/2} \cdot \left[\int_{X_0}^{X_N} A(X) \cdot S_S(X) \cdot \mathrm{d}X\right]^{1/2} \cdot \int_{X_0}^{X_N} A(X) \cdot \mathrm{d}X}{Q \cdot \Delta X \cdot \left[\int_{X0}^{X_N} P_w(X) \cdot \mathrm{d}X\right]^{1/2}}. \tag{6.39b}$$

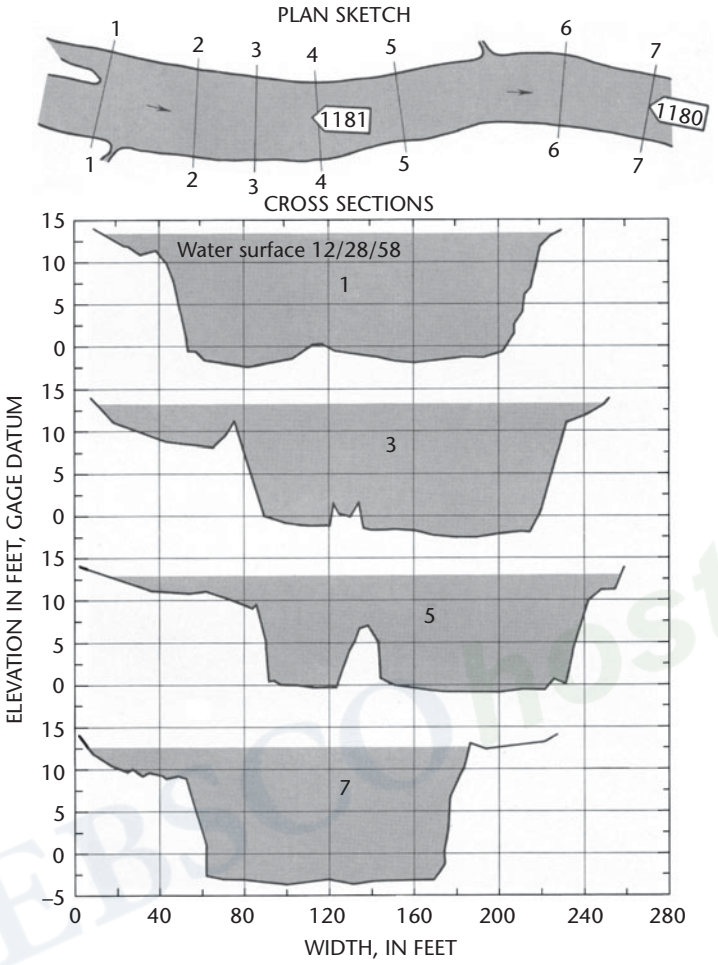

Figure 6.21 Plan view and cross sections of the Deep River at Ramseur, North Carolina, showing typical cross-section variability. From Barnes (1967).

In practice, the geometric functions $A(X)$, $S_S(X)$, and so on, can be approximated only by measurements at specific cross sections within the reach. Thus. for practical application, equation 6.39b becomes

$$\Omega = \frac{g^{1/2} \cdot \left[\sum_{i=1}^{N} A_i \cdot S_{Si} \cdot \Delta X_i \right]^{1/2} \cdot \sum_{i=1}^{N} A_i \cdot \Delta X_i}{Q \cdot \Delta X \cdot \left[\sum_{i=1}^{N} P_{wi} \cdot \Delta X_i \right]^{1/2}}, \tag{6.39c}$$

where the subscripts indicate the measured value of the variable at cross section i, $i = 1, 2, \ldots, N$, and ΔX_i is the downstream distance between successive cross sections.

Box 6.4 shows how field computations are used to compute resistance. It is important to be aware that careful field measurements are essential for accurate hydraulic computations. The manual by Harrelson et al. (1994) is an excellent illustrated guide to field technique.

6.8 The Manning Equation

6.8.1 Origin

In the century following the publication of the Chézy equation in 1769, European hydraulic engineers did considerable field and laboratory research to develop practical ways to estimate open-channel flow resistance (Rouse and Ince 1963; Dooge 1992). In 1889, Robert Manning (1816–1897), an Irish engineer, published an extensive review of that research (Manning 1889). He concluded that the simple equation that best fit the experimental results was

$$U = K_M \cdot R^{2/3} \cdot S_S^{1/2}, \tag{6.40a}$$

where K_M is a proportionality constant representing reach conductance. For historical reasons (see Dooge 1992), subsequent researchers replaced K_M by its inverse, $1/n_M$, and wrote the equation as

$$U = \left(\frac{1}{n_M}\right) \cdot R^{2/3} \cdot S_S^{1/2}, \tag{6.40b}$$

called **Manning's equation**, where the resistance factor n_M is called **Manning's *n***.

Manning's equation has come to be accepted as "the" resistance equation for open-channel flow, largely replacing the Chézy equation in practical applications. The essential difference between the two is that the hydraulic-radius exponent is 2/3 rather than 1/2. This difference is important because it makes the Manning equation dimensionally inhomogeneous.[8] As with Chézy's C (see box 6.1), values of n_M are treated as constants for all unit systems, and in order to give correct results, the Manning equation must be written as

$$U = u_M \cdot \left(\frac{1}{n_M}\right) \cdot R^{2/3} \cdot S^{1/2}, \tag{6.40c}$$

where u_M is a unit-adjustment factor that takes the following values:

Unit system	u_M
Système Internationale	1.00
British	1.49
Centimeter-gram-second	4.64

BOX 6.4 Calculation of Resistance, Deep River at Ramseur, North Carolina

The channel-geometry values in the table below were measured by Barnes (1967) at seven cross sections on the Deep River at Ramseur, North Carolina, on 28 December 1958, when the flow was $Q = 235\ m^3/s$ (figure 6.21). Note that $i = 0$ for the upstreammost cross section, so $N+1$ sections are measured, defining N subreaches (table 6B4.1).

Table 6B4.1

Section, i	A_i (m^2)	R_i (m)	P_{wi} (m)	ΔX_i(m)	$\lvert\Delta Z_i\rvert$ (m)	$S_{Si} = \lvert\Delta Z_i\rvert/\Delta X_i$
0	230.0	3.29	69.8			
1	198.4	3.17	62.6	66.8	0.052	0.000776
2	198.6	2.85	69.8	66.5	0.015	0.000229
3	223.4	2.66	83.9	55.5	0.037	0.000659
4	191.6	2.42	79.1	56.4	0.061	0.001081
5	210.5	3.29	63.9	102.7	0.091	0.000890
6	188.3	3.17	59.4	80.8	0.073	0.000906

(The quantity $|\Delta Z_i|$ is the decrease in water-surface elevation between successive sections.)

To compute the resistance via equation 6.39c, we calculate the quantities in table 6B4.2 from the above data.

Table 6B4.2

Section, i	$A_i \cdot S_{Si} \cdot \Delta X_i (m^3)$	$A_i \cdot \Delta X_i$ (m^3)	$P_{wi} \cdot \Delta X_i (m^3)$
1	10.286	13,250	4178.9
2	3.029	13,202	4636.2
3	8.172	12,394	4656.5
4	11.681	10,805	4463.6
5	19.256	21,631	6569.4
6	13.779	15,215	4798.5
Sum	66.202	86,497	29,303.1

From the previous table, $\Delta X = \Sigma \Delta X_i = 428.7$ m. Substituting the appropriate values into 6.39c gives

$$\Omega = \frac{9.81^{1/2} \cdot [66.202]^{1/2} \cdot 86497}{235 \cdot 428.7 \cdot [29303.1]^{1/2}} = 0.128.$$

The Reynolds number for this flow, assuming kinematic viscosity $\nu = 1.5 \times 10^{-6}\ m^2/s$, is

$$Re = \frac{U \cdot R}{\nu} = \frac{1.15\ m/s \times 2.98\ m}{1.5 \times 10^{-6} m^2/s} = 2.28 \times 10^6.$$

Referring to figure 6.8, we see that this flow was well into the "fully rough" range and that the actual resistance $\Omega = 0.128$ was well above the baseline value $\Omega_* \approx 0.04$ given by equation 6.25.

From equations 6.12, 6.19, 6B1.3, and 6.40c, we see that

$$n_M = \frac{u_M \cdot R^{1/6} \cdot K_T^{1/2}}{g^{1/2}} = \frac{u_M \cdot R^{1/6}}{u_C \cdot C} = \frac{u_M \cdot R^{1/6} \cdot \Omega}{g^{1/2}}. \tag{6.41}$$

A major justification for using the Manning equation instead of the Chézy equation has been that, because n_M depends on the hydraulic radius, it accounts for relative submergence effects and tends to be more constant for a given reach (i.e., changes less as discharge changes) than is C. However, this reasoning may not be compelling, because we have seen that we can write the Chézy equation using Ω^{-1} instead of $u_C \cdot C$ (equation 6.19) and that Ω, in fact, depends in large measure on relative submergence (equation 6.24). Another reason for the popularity of the Manning equation is that a number of methods have been developed that provide expedient (i.e., "quick-and-dirty") estimates of the resistance coefficient n_M. These methods are discussed in the following section.

6.8.2 Determination of Manning's n_M

In order to apply the Manning equation in practical problems, one must be able to determine a priori values of n_M. An overview of approaches to doing this are listed in table 6.3 and briefly described in the following subsections.

6.8.2.1 Visual Comparison with Photographs

Table 6.4 summarizes publications that provide guidance for field determination of n_M by means of photographs of reaches in which n_M values have been determined by measurement for one or more discharges. The books by Barnes (1967) and Hicks and Mason (1991) are specifically designed to provide visual guidance for the field determination of n_M for in-bank flows in natural rivers. Examples from Barnes (1967) are shown in figure 6.22.

6.8.2.2 Tables of Typical n_M Values

Chow (1959) provides tables that give a range of appropriate n_M values for various types of human-made canals and natural channels; the portions of those tables covering natural channels are reproduced here in table 6.5.

6.8.2.3 Formulas That Account for Components of Reach Resistance

Cowan (1956) introduced a formula that allowed for explicit consideration of many of the factors that determine resistance (see section 6.6) in determining an appropriate n_M value:

$$n_M = (n_0 + n_1 + n_2 + n_3 + n_4) \cdot m_\zeta, \tag{6.42}$$

where n_0 is the base value for straight, uniform, smooth channel in natural material; n_1 is the factor for bed and bank roughness; n_2 is the factor for effect of

Table 6.3 General approaches to a priori estimation of Manning's n_M.

Approach	Comments	References
1. Visual comparison with photographs of channels for which n_M has been measured (see table 6.4)	Expedient method; subjective, dependent on operator experience; subject to considerable uncertainty	Faskin (1963), Barnes (1967), Arcement and Schneider (1989), Hicks and Mason (1991)
2. Tables of typical n_M values for reaches of various materials and types (see table 6.5)	Expedient method; subjective, dependent on operator experience; subject to considerable uncertainty	Chow (1959), French (1985)
3. Formulas that account for components of reach resistance (see table 6.6)	Expedient method; more objective than approaches 1 and 2 but lacks theoretical basis	Cowan (1956), Faskin (1963), Arcement and Schneider (1989)
4. Formulas that relate n_M to bed-sediment grain size d_p (see table 6.7)	Require measurement of bed sediment; reliable only for straight quasi-prismatic channels where bed roughness is the dominant factor contributing to resistance	Chang (1988), Marcus et al. (1992)
5. Formulas that relate n_M to hydraulic radius and relative smoothness	Require measurement of bed sediment, depth, and slope; forms are based on theory; coefficients are based on field measurement; can give good results in conditions similar to those for which established	Limerinos (1970), Bathurst (1985)
6. Statistical formulas that relate n_M to measurable flow parameters (see table 6.8)	Can provide good estimates, especially useful when bed-material information is lacking, as in remote sensing, but subject to considerable uncertainty	Riggs (1976), Jarrett (1984), Dingman and Sharma (1997), Bjerklie et al. (2003)

Table 6.4 Summary of reports presenting photographs of reaches for which Manning's n_M has been measured.

Types of reach	No. of reaches	No. of flows	Minimum n_M	Maximum n_M	Reference
Canals and dredged channels (USA)	48	326	0.014	0.162	Faskin (1963)
Natural rivers (USA)	51	62	0.024	0.075	Barnes (1967)
Flood plains (USA)	16	16	—[a]	—[a]	Arcement and Schneider (1989)
Natural rivers (New Zealand)	78	559	0.016	0.270	Hicks and Mason (1991)

[a] See reference for methodology for computing composite (channel plus flood plain) n_M values.

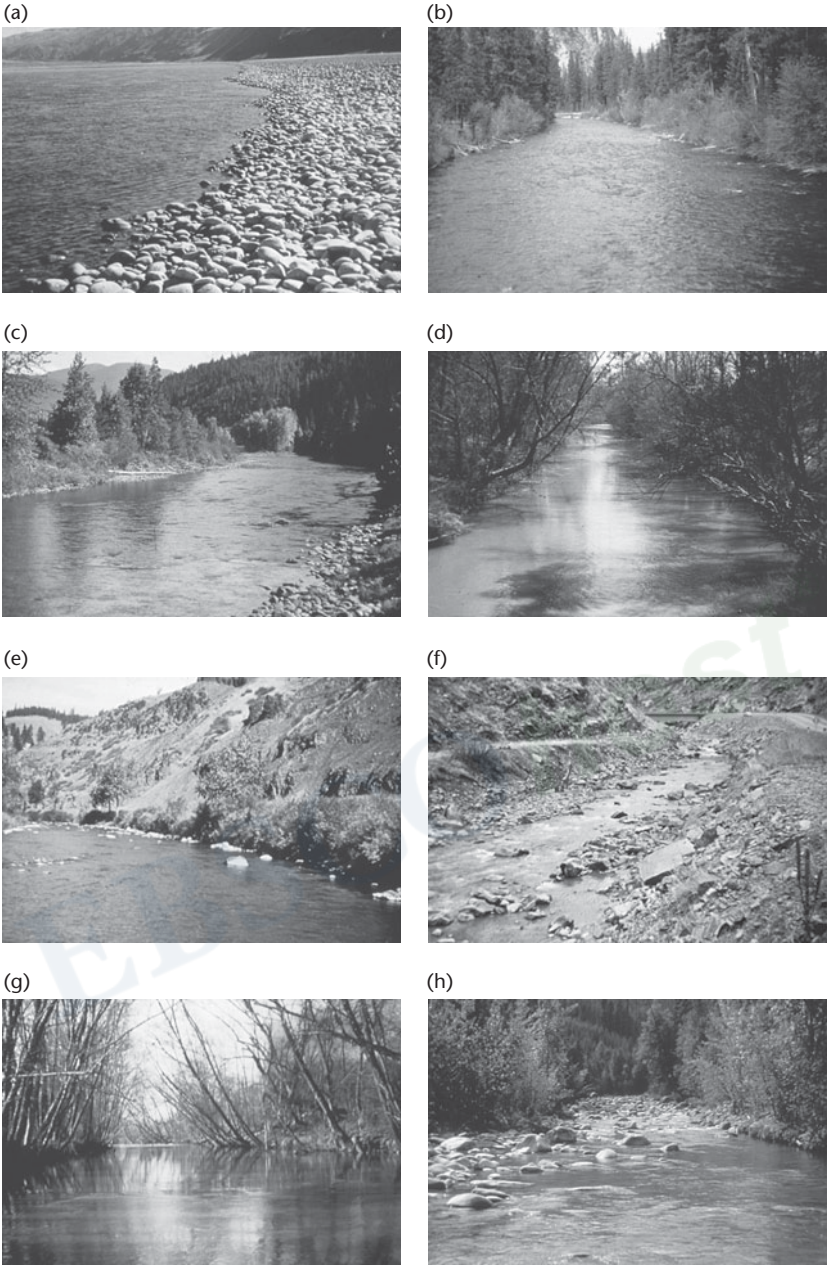

Figure 6.22 Photographs of U.S. river reaches covering a range of values of Manning's n_M, computed from measurements. (a) Columbia River at Vernita, Washington: $n_M = 0.024$; (b) West Fork Bitterroot River near Conner, Montana: $n_M = 0.036$; c) Moyie River at Eastport, Idaho: $n_M = 0.038$; (d) Tobesofkee Creek near Macon, Georgia: $n_M = 0.041$; (e) Grande Ronde River at La Grande, Oregon: $n_M = 0.043$; (f) Clear Creek near Golden, Colorado: $n_M = 0.050$; (g) Haw River near Benaja, North Carolina: $n_M = 0.059$; (h) Boundary Creek near Porthill, Idaho: $n_M = 0.073$. From Barnes (1967); photographs courtesy U.S. Geological Survey.

Table 6.5 Values of Manning's n_M for natural streams.

Channel description	Minimum	Normal	Maximum
Minor streams (bankfull width < 100 ft)			
Streams on plain			
1. Clean, straight, full stage, no riffles or deep pools	0.025	0.030	0.033
2. Same as above, but more stones and weeds	0.030	0.035	0.040
3. Clean, winding, some pools and shoals	0.033	0.040	0.045
4. Same as above, but some weeds and stones	0.035	0.045	0.050
5. Same as above, but lower stages, more ineffective slopes and sections	0.040	0.048	0.055
6. Same as item 4, but more stones	0.045	0.050	0.060
7. Sluggish reaches, weedy, deep pools	0.050	0.070	0.080
8. Very weedy reaches, deep pools, or floodways with heavy stand of timber and underbrush	0.075	0.100	0.150
Mountain Streams			
No vegetation in channel, banks usually steep, trees and brush along banks submerged at high stages			
1. Bottom: gravels, cobbles, and few boulders	0.030	0.040	0.050
2. Bottom: cobbles with large boulders	0.040	0.050	0.070
Major Streams (bankfull width > 100 ft)			
1. Regular section with no boulders or brush	0.025	—	0.060
2. Irregular and rough section	0.035	—	0.100
Floodplains			
1. Short grass, no brush	0.025	0.030	0.035
2. High grass, no brush	0.030	0.035	0.050
3. Cultivated area, no crop	0.020	0.030	0.040
4. Mature row crops	0.025	0.035	0.045
5. Mature field crops	0.030	0.040	0.050
6. Scattered brush, heavy weeds	0.035	0.050	0.070
7. Light brush and trees, in winter	0.035	0.050	0.060
8. Light brush and trees, in summer	0.040	0.060	0.080
9. Medium to dense brush, in winter	0.045	0.070	0.110
10. Medium to dense brush, in summer	0.070	0.100	0.160
11. Dense willows, summer, straight	0.110	0.150	0.200
12. Cleared land with tree stumps, no sprouts	0.030	0.040	0.050
13. Same as above, but with heavy growth of sprouts	0.050	0.060	0.080
14. Heavy stand of timber, a few down trees, little undergrowth, flood stage below branches	0.080	0.100	0.120
15. Same as above, but with flood stage reaching branches	0.100	0.120	0.160

From Chow (1959, table 5.6). Reproduced with permission of McGraw-Hill.

cross-section irregularity; n_3 is the factor for the effect of obstructions; n_4 is the factor for vegetation and flow conditions; and m_ζ is the factor for sinuosity. Table 6.6 summarizes the determination of values for these factors.

Although equation 6.42 may provide a somewhat more objective method for considering the various factors that affect resistance than simply referring to tables or figures, note that there is no theoretical basis for assuming that n_M values are simply additive.

Table 6.6 Values of factors for estimating n_M via Cowan's (1956) formula (equation 6.42).

Material	n_0
Concrete	0.011–0.018
Rock cut	0.025
Firm soil	0.020–0.032
Sand ($d = 0.2$ mm)	0.012
Sand ($d = 0.5$ mm)	0.022
Sand ($d = 1.0$ mm)	0.026
Sand ($1.0 \leq d \leq 2.0$ mm)	0.026–0.035
Gravel	0.024–0.035
Cobbles	0.030–0.050
Boulders	0.040–0.070
Degree of Irregularity	n_1
Smooth	0.000
Minor	0.001–0.005
Moderate	0.006–0.010
Severe	0.011–0.020
Cross-Section Irregularity	n_2
Gradual	0.000
Alternating occasionally	0.001–0.005
Alternating frequently	0.010–0.015
Obstructions	n_3
Negligible	0.000–0.004
Minor	0.005–0.015
Appreciable	0.020–0.030
Severe	0.040–0.050
Amount of Vegetation	n_4
Small	0.002–0.010
Medium	0.010–0.025
Large	0.025–0.050
Very large	0.050–0.100
Sinuosity, ζ	m_ζ
$1.0 \leq \zeta \leq 1.2$	1.00
$1.2 \leq \zeta \leq 1.5$	1.15
$1.5 \leq \zeta$	1.30

6.8.2.4 *Formulas That Relate n_M to Bed-Sediment Size and Relative Smoothness*

From a study of flows over uniform sands and gravels, Strickler (1923) proposed that n_M is related to bed-sediment size as

$$n_M = 0.0150 \cdot d_{50}(mm)^{1/6}, \tag{6.43a}$$

where d_{50} is median grain diameter in mm, or

$$n_M = 0.0474 \cdot d_{50}(m)^{1/6}, \tag{6.43b}$$

where d_{50} is median grain diameter in m. Formulas of this form are called **Strickler formulas**, and several versions have been proffered by various researchers (see table 6.7). Although Strickler-type formulas are often invoked, experience shows that n_M values computed for natural channels from bed sediment alone are usually smaller than actual values.

It is interesting to note that, using equation 6.43b, the Manning equation (equation 6.40c) can be written as

$$U = 6.74 \cdot \left(\frac{R}{d_{50}}\right)^{1/6} \cdot u_* = 6.74 \cdot \left(\frac{R}{d_{50}}\right)^{0.167} \cdot (g \cdot Y \cdot S_S)^{1/2}; \tag{6.44}$$

which can be interpreted as an integrated 1/6-power-law velocity profile (see equation 5.46 with $m_{\mathrm{PL}} = 1/6$). This equation is of the same form as equation 4.74, which was developed from dimensional analysis and measured values, but has a considerably different coefficient (1.84) and exponent (0.704).

We have seen several formulas (equations 6.25, 6.27, 6.28, 6.30, and 6.32) that relate resistance in fully rough flows to relative roughness in the form

$$\Omega = \kappa \cdot \left[-\ln\left(\frac{y_r}{K_r \cdot R}\right)\right]^{-1}, \tag{6.45}$$

Table 6.7 Formulas relating Manning's n_M to bed-sediment size and relative smoothness (grain diameters d_p, in mm; hydraulic radius, R, in m).

Formula	Remarks	Source
n_M or $n_0 = 0.015 \cdot d^{1/6}$	Original "Strickler formula" for uniform sand	Strickler (1923) as reported by Chang (1988)
n_M or $n_0 = 0.0079 \cdot d_{90}^{1/6}$		Keulegan (1938) as reported by Marcus et al. (1992)
n_M or $n_0 = 0.0122 \cdot d_{90}^{1/6}$	Sand mixtures	Meyer-Peter and Muller (1948)
n_M or $n_0 = 0.015 \cdot d_{75}^{1/6}$	Gravel lined canals	Lane and Carlson (1938) as reported by Chang (1988)
n_M or $n_0 = \dfrac{R^{1/6}}{[7.69 \cdot \ln(R/d_{84}) + 63.4]}$		Limerinos (1970)
n_M or $n_0 = \dfrac{R^{1/6}}{[7.64 \cdot \ln(R/d_{84}) + 65.3]}$	Gravel streams with slope > 0.004	Bathurst (1985)
n_M or $n_0 = \dfrac{R^{1/6}}{[7.83 \cdot \ln(R/d_{84}) + 72.9]}$	Derived from P-vK law for wide channels	Dingman (1984)

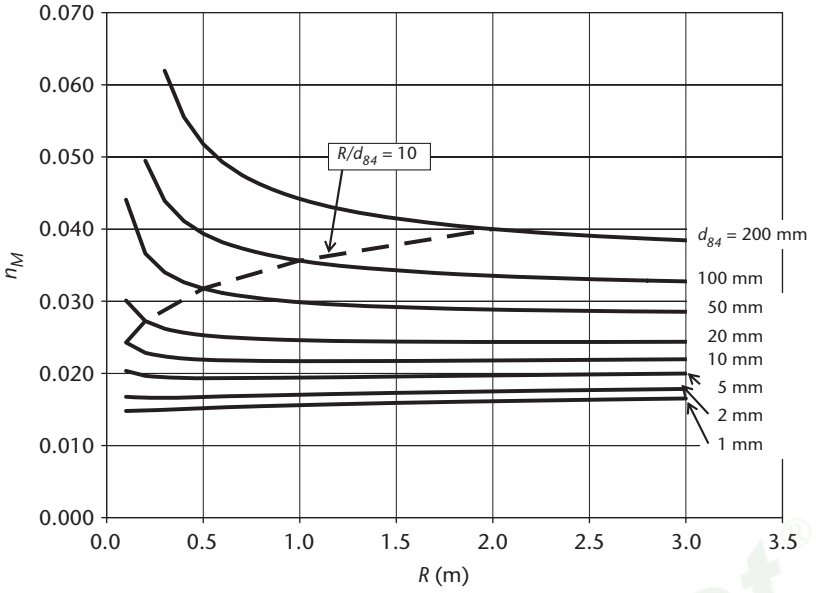

Figure 6.23 Variation of Manning's n_M (or n_0 in equation 6.42) with hydraulic radius, R, and bed grain diameter d_{84} as predicted by the Dingman (1984) version of equation 6.46 (see table 6.7). Manning's n_M is effectively independent of depth for $R/d_{84} > 10$.

where the values of κ, K_r, and y_r take different values in different contexts. If equation 6.45 is substituted into equation 6.41, we find that

$$n_M = \frac{u_M \cdot \kappa \cdot R^{1/6}}{g^{1/2} \cdot \ln\left(\frac{K_r \cdot R}{y_r}\right)}. \tag{6.46}$$

Thus, equation 6.46 can be used to provide estimates of n_M (or n_0 in equation 6.42) in those contexts. Table 6.7 lists versions of equation 6.46 derived by various authors, and figure 6.23 shows the relation of n_M to relative smoothness for various bed-sediment sizes in gravel-bed streams as given by the Dingman (1984) version of that equation. Note that the formula predicts little dependence of n_M on R/d_{84} when $R/d_{84} > 10$.

6.8.2.5 *Statistically Derived Formulas That Relate n_M to Hydraulic Variables*

A number of researchers have used statistical analysis (regression analysis, as described in section 4.8.3.1) to develop equations to predict n_M based on measurable flow variables. Three of these equations are listed in table 6.8. There is considerable uncertainty associated with estimates from such equations: The equation of Dingman and Sharma (1997), which is based on the most extensive data set, was found to give

Table 6.8 Statistically derived formulas for estimating Manning's n_M [A = cross-sectional area (m^2); R = hydraulic radius (m); S =slope].

Formula	Remarks	Source
$n_M = 0.210 \cdot A^{-0.33} \cdot R^{0.667} \cdot S^{0.095}$	Based on 62 flows in Barnes (1967); $0.024 \leq n_M \leq 0.075$	Riggs (1976)
$n_M = 0.32 \cdot R^{-0.16} \cdot S^{0.38}$	Mountain streams with 0.17 m $\leq R \leq$ 2.13 m and $0.002 \leq S \leq 0.052$	Jarrett (1984)
$n_M = 0.217 \cdot A^{-0.173} \cdot R^{0.267} \cdot S^{0.156}$	Based on 520 flows from Hicks and Mason (1991); $0.015 \leq n_M \leq 0.290$	Dingman and Sharma (1997)

discharge estimates within ±50% of the true value 77% of the time. This topic is addressed further in section 6.9.

6.8.2.6 *Field Measurement of Discharge and Hydraulic Variables*

The only way that the value of Manning's n_M can be established with certainty is by measuring the discharge and hydraulic variables at a given time in a given reach, determining the prevailing reach-average velocity, and solving the Manning equation for n_M. Ideally, one would repeat the calculations over a range of discharges in a particular reach and use the n_M values so determined in future a priori estimates of velocity or discharge for that reach.

Barnes (1967) and Hicks and Mason (1991) give equations for direct computation of n_M from measured values of discharge and surveyed values of cross-sectional area, hydraulic radius, reach length, and water-surface slope at several cross sections within a reach. However, their methodology is based on energy considerations (sections 4.5 and 8.1), whereas the Manning equation is a modification of the Chézy equation, which was derived from momentum considerations (sections 4.4 and 8.2).[9] Thus, it is preferable to compute resistance via the method described in section 6.7 for computing Ω (equation 6.39c); if desired, the corresponding n_M value can then be determined via equation 6.41. In most cases, the two methods give very similar n_M values (within ±0.002).

6.8.3 Summary

As noted above, the Manning equation has been the most commonly used resistance relation for most engineering and many scientific purposes. It is common to use the expedient methods described in approaches 1–3 of table 6.3 to estimate n_M in these applications. However, it has been shown that even engineers with extensive field experience generate a wide range of n_M estimates for a given reach using these methods (Hydrologic Engineering Center 1986). Approach 4 is not usually appropriate for natural rivers because, as we have seen, resistance depends on many factors in addition to bed material. The various equations developed for approach 5 can be used for conditions similar to those for which the particular equation was established. Approach 6 can be useful, especially when trying to estimate discharge

via remote sensing (Bjerklie et al. 2003), but may produce errors of ±50% or more (see section 6.9). As noted above, the only way to determine resistance (Ω or n_M) with certainty for a given reach is to measure discharge and reach-average values of hydraulic variables at a given discharge and use equation 6.39c and, if desired, equation 6.41.

The questionable theoretical basis for the Manning equation—reflected in its dimensional inhomogeneity—and the common reliance on expedient methods for estimating n_M significantly limit the confidence one can have in many applications of the Manning equation. As explained in section 6.3, the Chézy equation has a theoretical basis and, coupled with 1) the theoretical and empirical studies of resistance summarized in the Moody diagram (figure 6.8) and 2) the various studies described in sections 6.5 and 6.6, provides a sound and useful framework for understanding and estimating reach resistance. Thus, there seems to be no well-founded theoretical or empirical basis for preferring the Manning equation to the Chézy equation. However, as we will see in the following section, the theoretical basis for the Chézy equation may itself need reexamination.

6.9 Statistically Derived Resistance Equations

Because of the theoretical uncertainty associated with the Manning equation and the difficulty of formulating physically based approaches for characterizing resistance, some researchers have applied statistical techniques (regression analysis, section 4.8.3.1) to identify relations between discharge or velocity and other measurable hydraulic variables (Golubtsev 1969; Riggs 1976; Jarrett 1984; Dingman and Sharma 1997).

Box 6.5 describes a study that compares the performance of five statistically established resistance/conductance models for a large set of flow data. Overall, the study found that the best predictor was the "modified Manning" model:

$$Q = 7.14 \cdot W \cdot Y^{5/3} \cdot S_0^{1/3}, \tag{6.47}$$

where Q is discharge (m^3/s), W is width (m), Y is average depth (m), and S_0 is channel slope.

Interestingly, that study found that resistance models incorporating a slope exponent $q = 1/3$ (the "modified Manning" and "modified Chézy," as well as the pure regression relation) had greater predictive accuracy than those using the generally accepted theoretical value $q = 1/2$. A possible interpretation of this result is that the assumption that resistance (shear stress) is proportional to the square of velocity (equation 6.8), which is the basis of the derivation of the Chézy resistance relation, is not completely valid.

Measurements of resistance/conductance (e.g., Barnes 1967; Hicks and Mason 1991) clearly demonstrate that resistance varies strongly from reach to reach and with varying discharge in a given reach. The Bjerklie et al. (2005b) study in fact found that values of K_2 (equation 6B5.2a) for individual flows varied from about 1.0 to as high as 18, with about two-thirds of the values Between 4.6 and 9.6. Thus, the use of a universal conductance coefficient as in 6.47 is not correct.

BOX 6.5 Statistically Determined Resistance/Conductance Equations

Bjerklie et al. (2005b) used data for 1037 flows at 103 reaches to compare four resistance/conductance models incorporating various combinations of depth exponents and slope exponents.

Manning model:

$$Q = K_1 \cdot W \cdot Y^{5/3} \cdot S_0^{1/2} \qquad \text{(6B5.1a)}$$

Modified Manning model:

$$Q = K_2 \cdot W \cdot Y^{5/3} \cdot S_0^{1/3} \qquad \text{(6B5.2a)}$$

Chézy model:

$$Q = K_3 \cdot W \cdot Y^{3/2} \cdot S_0^{1/2} \qquad \text{(6B5.3a)}$$

Modified Chézy model

$$Q = K_4 \cdot W \cdot Y^{3/2} \cdot S_0^{1/3} \qquad \text{(6B5.4a)}$$

In these models, Q is discharge, $K_1 - K_4$ are conductance coefficients, W is width, Y is average depth, and S_0 is channel slope. These models can also be written as velocity predictors by dividing both sides by $W \cdot Y$.

The best-fit values of $K_1 - K_4$ were determined by statistical analysis of 680 of the flows.

Manning model:

$$Q = 23.3 \cdot W \cdot Y^{2/3} \cdot S_0^{1/2} \qquad \text{(6B5.1b)}$$

Modified Manning model:

$$Q = 7.14 \cdot W \cdot Y^{5/3} \cdot S_0^{1/3} \qquad \text{(6B5.2b)}$$

Chézy model:

$$Q = 25.2 \cdot W \cdot Y^{3/2} \cdot S_0^{1/2} \qquad \text{(6B5.3b)}$$

Modified Chézy model:

$$Q = 7.73 \cdot W \cdot Y^{3/2} \cdot S_0^{1/3} \qquad \text{(6B5.4b)}$$

SI units were used for all quantities. A fifth resistance model was determined by log-regression analysis (section 4.8.3.1) of the 680 flows.

Regression model:

$$Q = 4.84 \cdot W^{1.10} \cdot Y^{1.63} \cdot S_0^{0.330} \qquad \text{(6B5.5)}$$

Note that the statistically determined exponent values in equation 6B5.5 are close to those of the "modified Manning" model (equation 6B5.2).

The predictive ability of these five equations was then compared for the 357 flows not used to establish the numerical values of $K_1 - K_4$ and equation 6B5.5 using several criteria. Overall, the "modified Manning" relation performed best, and the study found that resistance models incorporating a slope exponent $q = 1/3$ (the modified Manning and modified Chézy, as well as the pure regression relation) had greater predictive accuracy than those using the generally accepted theoretical value $q = 1/2$. For all models, there was a strong relation between prediction error and Froude number, *Fr*: The models tended to overestimate discharge for $Fr <\sim 0.15$, and underestimate for $Fr > 0.4$. Unfortunately, this information cannot be used to improve the predictions, because one needs to know velocity to compute *Fr*.

However, given the theoretical difficulties in characterizing resistance/conductance and the need to estimate discharge for cases where there is little or no reach-specific information available, "universal" equations such as 6.47 may be useful. This is particularly true attempting to estimate discharge from satellite or airborne remote-sensing information (Bjerklie et al. 2003). The statistical results (i.e., the suggestion that $q = 1/3$ rather than 1/2) may also point to a reexamination of some of the theoretical assumptions underlying the phenomenon of reach resistance—or to the fact that many natural flows are far from uniform.

6.10 Applications of Resistance Equations

As stated at the beginning of this chapter, the central problem of open-channel-flow hydraulics can be stated as that of determining the average velocity (or depth) associated with a specified discharge in a reach with a specified geometry and bed material. Two practical versions of that problem that commonly arise are:

1. Given a range of discharges due to hydrological processes upstream of the reach, what average velocity and depth will be associated with each discharge? Answers to this question provide information about the elevation and areal extent of flooding to be expected at future high discharges, the ability of the river to assimilate wastes, the amount of erosion to be expected at various discharges, and the suitability of riverine habitats at various discharges. These answers are in the form of reach-specific functions $U = f_U(Q)$ and/or $Y = f_Y(Q)$, where Q is discharge.
2. Given evidence of the water-surface elevation for a recent flood, what was the flood discharge? Answers to this question are important in determining regional flood magnitude–frequency relations. The answers may be expressed functionally as $Q = f_Q(Y)$.

This section shows how these problems are approached for a reach in which concurrent measurements of discharge and hydraulic parameters are not available, but where it

is possible to obtain measurements of channel geometry, channel slope, and bed material.

Although both types of problems commonly arise in situations involving overbank flow on floodplains, the discussion here applies when flow is contained within the channel banks. When flow extends onto the floodplain, the channel and the floodplain usually have very different resistances, and the cross section is **compound**. Methods for treating flows in reaches with compound sections are discussed in Chow (1959), French (1985), and Yen (2002).

6.10.1 Determining the Velocity–Discharge and Depth–Discharge Relations

Box 6.6 summarizes the steps involved in determining velocity–discharge and depth–discharge relations for an ungaged reach. The process begins with a survey of channel geometry (boxes 2.1 and 2.2); this is demonstrated in box 6.7 for the Hutt River

BOX 6.6 Steps for Estimating Velocity–Discharge and Depth–Discharge Relations for an Ungaged Reach

1. Using the techniques of box 2.1, identify the bankfull elevation through the reach.
2. Using the techniques of box 2.2 [1. Channel (Bankfull) Geometry], survey a typical cross section to determine the channel geometry.
3. Determine the size distribution of bed sediment, d_p. [See section 2.3.2.1. Refer to Bunte and Abt (2001) for detailed field procedures.]
4. Survey water-surface elevation through the reach to determine water-surface slope, S_S. [Refer to Harrelson et al. (1994) for detailed survey procedures.]
5. Select a range of elevations up to bankfull.
6. Using the techniques of box 2.2 (2. Geometry at a Subbankfull Flow), determine water-surface width W, cross-sectional area A, and average depth $Y \equiv A/W$ associated with each selected elevation.
7. Estimate reach resistance: (a) If using the Chézy equation, use results of steps 3–6 to estimate Ω_* via equation 6.25 for each selected elevation and adjust to give Ω based on considerations of section 6.6. (b) If using the Manning equation, use one of the methods of section 6.8.2 to estimate Manning's n_M.
8. Assume hydraulic radius $R = Y$ and estimate average velocity U for each selected elevation via either the Chézy equation (equation 6.15a) or the Manning equation (equation 6.40).
9. Estimate discharge as $Q = U \cdot A$ for each selected elevation.
10. Use results to generate plots of U versus Q and Y versus Q.

BOX 6.7 Example Computation of Channel Geometry: Hutt River at Kaitoke, New Zealand

The line of a cross section is oriented at right angles to the general flow direction. An arbitrary zero point is established at one end of the line; by convention, this is usually on the left bank (facing downstream), but it can be on either bank. Points are selected along the line to define the cross-section shape; these are typically "slope breaks"—points where the ground-surface slope changes. An arbitrary elevation datum is established, and the elevations of these points above this datum are determined by surveying (see Harrelson et al. 1994). To illustrate the computations, we use data for a cross section of the Hutt River in New Zealand (figure 6.24). Section survey results are recorded as elevations, z_i, at distances along the section line, w_i. At each point, the local bankfull depth Y_{BFi} can be calculated as

$$Y_{BFi} = \Psi_{BF} - z_i, \tag{6B7.1}$$

where Ψ_{BF} is the bankfull maximum depth. The data for the Hutt River section are given in table 6B7.1 and are plotted in figure 6.25.

Table 6B7.1

$\mathbf{w}_i$ (m)	0.0	1.0	5.5	7.5	9.0	10.0	11.2	13.3	13.4	14.5
$\mathbf{z}_i$ (m)	3.78	3.71	2.72	2.18	1.92	1.50	0.96	0.86	0.85	0.54
Y_{BFi} (m)	0.00	0.07	1.06	1.60	1.86	2.28	2.82	2.92	3.13	3.24
$\mathbf{w}_i$ (m)	17.5	19.8	19.9	20.6	21.3	24.0	25.8	27.7	28.8	30.0
$\mathbf{z}_i$ (m)	0.53	0.58	0.32	0.28	0.41	0.30	0.44	0.12	0.00	0.24
Y_{BFi} (m)	3.25	3.20	3.46	3.50	3.37	3.49	3.34	3.66	3.78	3.54
$\mathbf{w}_i$ (m)	32.3	34.3	35.1	38.4	39.9	41.2	42.5	43.5	44.8	45.0
$\mathbf{z}_i$ (m)	0.23	0.29	0.50	0.64	0.80	1.84	2.41	2.90	3.71	3.78
Y_{BFi} (m)	3.55	3.49	3.28	3.14	2.98	1.94	1.37	0.88	0.07	0.00

Once the section is plotted, several arbitrary elevations are identified to represent water-surface elevations (the horizontal lines in figure 6.25). For each level, the horizontal positions of the left- and right-bank intersections of the level line with the channel bottom are determined and identified as w_L and w_R, respectively. For each selected elevation, the water-surface width W is

$$W = |w_R - w_L|. \tag{6B7.2}$$

Selecting the level $\Psi = 2$ m in the Hutt River cross section for example calculations, we see from figure 6.25 that

$$W = |41.5 - 8.5| = 33.0 \text{ m}.$$

(*Continued*)

BOX 6.7 *Continued*

The cross-sectional area A associated with a given level is found as

$$A = \sum_{i=1}^{N} A_i = \sum_{i=1}^{N} W_i \cdot Y_i, \tag{6B7.3}$$

where W_i is the incremental width associated with each surveyed depth Y_i, N is the number of points for which we have observations, and $i = 1, 2, \ldots, N$. If we start from the left bank, $W_1 = w_L$, $W_N = w_R$, and $Y_1 = 0$, $Y_N = 0$ in all cases. The values of the incremental widths are determined as

$$W_1 = \frac{|w_2 - w_1|}{2}; \tag{6B7.4a}$$

$$W_i = \frac{|w_{i+1} - w_{i-1}|}{2}, i = 2, 3, \ldots, N-1; \tag{6B7.4b}$$

$$W_N = \frac{|w_N - w_{N-1}|}{2}. \tag{6B7.6c}$$

Note that $\Sigma W_i = W$.

Table 6B7.2 gives the data for the $\Psi = 2$ m elevation in the Hutt River cross section.

Table 6B7.2

i	w_i(m)	Y_i(m)	W_i(m)	A_i(m^2)
1	8.5	0.00	0.25	0.000
2	9.0	0.08	0.75	0.063
3	10.0	0.50	1.10	0.553
4	11.2	1.04	1.65	1.721
5	13.3	1.14	1.10	1.253
6	13.4	1.35	0.60	0.809
7	14.5	1.46	2.05	2.999
8	17.5	1.47	2.65	3.903
9	19.8	1.42	1.20	1.708
10	19.9	1.68	0.40	0.671
11	20.6	1.72	0.70	1.206
12	21.3	1.59	1.70	2.701
13	24.0	1.71	2.25	3.836
14	25.8	1.56	1.85	2.882
15	27.7	1.88	1.50	2.817
16	28.8	2.00	1.15	2.300
17	30.0	1.76	1.75	3.080
18	32.3	1.77	2.15	3.812
19	34.3	1.71	1.40	2.395
20	35.1	1.50	2.05	3.073
21	38.4	1.36	2.40	3.257
22	39.9	1.20	1.40	1.680
23	41.2	0.16	0.80	0.130
24	41.5	0.00	0.15	0.000
Sum			$33.00 = W$	$46.851 = A$

The average depth, Y, associated with this elevation is

$$Y \equiv \frac{A}{W}, \tag{6B7.5}$$

so for the example calculation,

$$Y = \frac{46.851}{33.0} = 1.42 \text{ m}.$$

These computations are repeated for each of the selected elevations.

in New Zealand (figures 6.24 and 6.25). The construction of the velocity–discharge and depth–discharge relations is demonstrated for the Hutt River in box 6.8; the results are shown in figure 6.26.

6.10.2 Determining Past Flood Discharge (Slope-Area Measurements)

As noted above, knowledge of past flood discharges in reaches where discharge is not measured is helpful in understanding regional flood-frequency relations. A flood wave passing through a reach typically leaves evidence of the maximum water level in the form of scour marks, removal of leaves and other vegetative material, and/or deposition of silt. Where such evidence is present one can survey the flow cross sections at locations through the reach and estimate the peak flood discharge by inverting equation 6.39c:

$$Q = \frac{g^{1/2} \cdot \left[\sum_{i=1}^{N} A_i \cdot S_i \cdot \Delta X_i \right]^{1/2} \cdot \sum_{i=1}^{N} A_i \cdot \Delta X_i}{\Omega \cdot \Delta X \cdot \left[\sum_{i=1}^{N} P_{wi} \cdot \Delta X_i \right]^{1/2}} \tag{6.48}$$

This a posteriori application of the resistance relation is called a **slope-area computation**.

The critical practical issue in slope-area computations is in determining the appropriate value of Ω. The standard approach is to use the Manning equation after determining n_M via one of the methods described in section 6.8.2; one can then compute Ω via equation 6.41 or compute Q directly via the Manning equation.

Box 6.9 illustrates the application of equation 6.48 in a slope-area computation, first using a resistance estimated using one of the formulas based on grain size and relative smoothness, and then using a resistance measured in the reach at a lower flow. In this case, the discharge using the estimated resistance was several times too

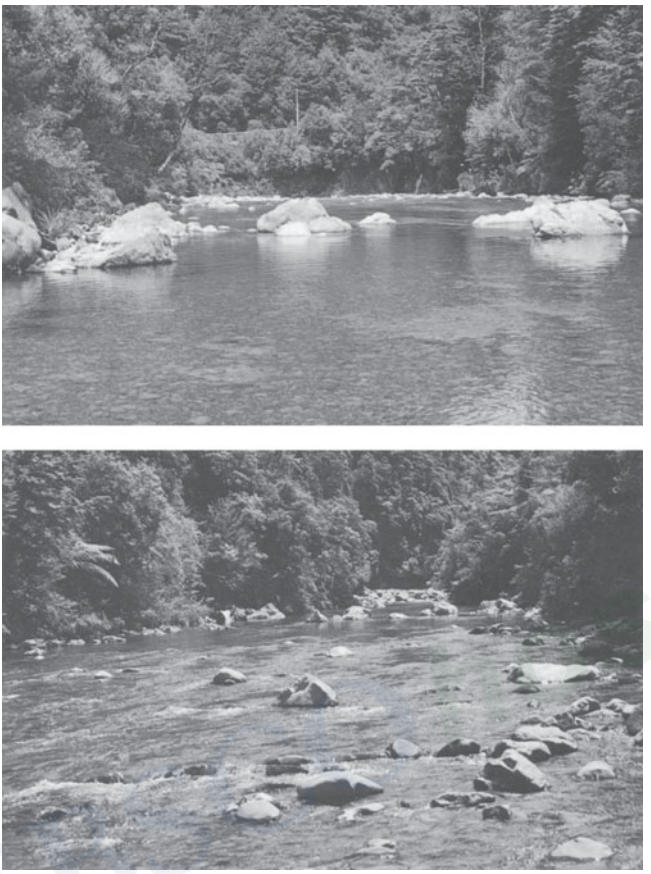

Figure 6.24 The Hutt River at Kaitoke, New Zealand. (a) View downstream at middle of reach. (b) View upstream at middle of reach. From Hicks and Mason (1991); reproduced with permission of New Zealand National Institute of Water and Atmospheric Research Ltd.

large (i.e., resistance was severely underestimated), while the discharge using the measured resistance was within 2% of the actual value. However, such good results may not always be obtained even with resistance values measured in the reach of interest, because one or more of the factors discussed in section 6.6 may have been significantly different at the time of the peak flow than at the time of measurement (Kirby 1987):

Cross-section geometry: The peak flow may have scoured the channel bed and subsequent lower flows deposited bed sediment. If this happened, the cross-sectional area that existed at the time of the peak flow was larger than the surveyed values and the peak discharge will be underestimated.

Plan-view irregularity: In meandering streams, high flows may "short-circuit" the bends, leading to lower resistance at the high flow than when measured at lower flows.

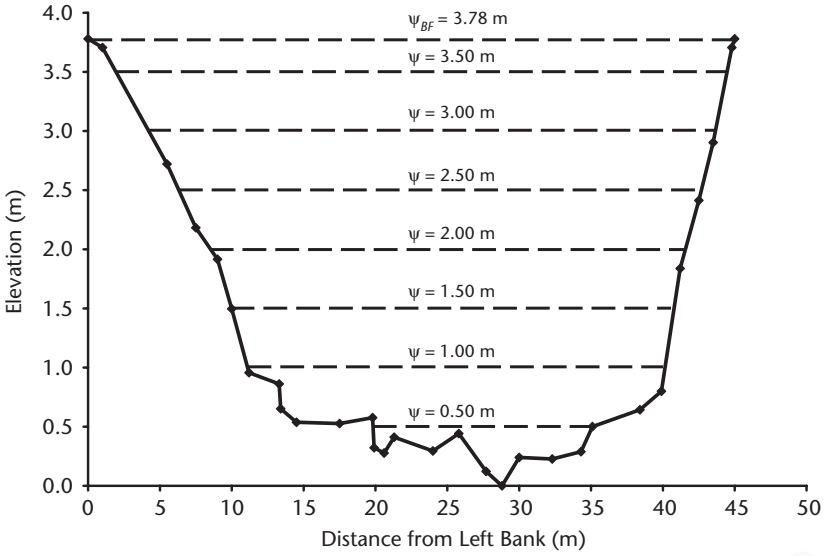

Figure 6.25 Surveyed cross section in the center of the Hutt River reach shown in figure 6.24. Elevations are relative to the lowest elevation in the cross section. The dashed lines are the water levels at the maximum depths (Ψ) indicated; Ψ_{BF} is the bankfull maximum depth. Note approximately 10-fold vertical exaggeration.

BOX 6.8 Example Computation of Velocity–Discharge and Depth–Discharge Relations for an Ungaged Reach: Hutt River at Kaitoke, New Zealand

Using the procedure described in boxes 6.6 and 6.7, the following values of average depth Y have been computed for selected maximum-depth levels Ψ for the cross section of the Hutt River at Kaitoke, New Zealand, shown in figure 6.25:

Ψ (m)	0.50	1.00	1.50	2.00	2.50	3.00	3.50	3.78
Y **(m)**	0.22	0.55	1.01	1.42	1.77	2.11	2.44	2.57

The bed-sediment material consists of gravel, cobbles, and boulders; $d_{84} =$ 212 mm. The average channel slope through the reach is $S = 0.00539$. We estimate the velocity–discharge and depth–discharge relations for this cross section via 1) the Chézy equation and 2) the Manning equation.

Chézy Equation

There is a range of bed-material sizes; we select the resistance relation for gravel-bed streams suggested by Bathurst (1993) (equation 6.27).

(Continued)

BOX 6.8 *Continued*

We assume $R = Y$ and estimate Ω as

$$\Omega = 0.400 \cdot \left[-\ln\left(\frac{0.212}{3.60 \cdot R}\right)\right]^{-1}.$$

Values of u_* are determined via equation 6.16:

$$u_* = (9.81 \cdot R \cdot 0.00539)^{1/2}$$

Average velocity U is then computed via equation 6.19 and discharge Q via equation 6.3. The results are tabulated in table 6B8.1.

Table 6B8.1

Ψ (m)	0.50	1.00	1.50	2.00	2.50	3.00	3.50	3.78
R (m)	0.22	0.55	1.01	1.42	1.77	2.11	2.44	2.57
Ω	0.301	0.179	0.141	0.126	0.118	0.112	0.107	0.106
U (m/s)	0.359	0.956	1.642	2.180	2.603	2.988	3.344	3.480
Q (m^3/s)	1.19	15.3	50.9	102	167	249	348	404

Manning Equation

In practice, one would use one of the approaches listed in table 6.3 and discussed in section 6.8.2 to estimate the appropriate n_M for this reach. In this example, we will use the value determined for the reach by measurement and reported in Hicks and Mason (1991): $n_M = 0.037$. Using this value and the measured slope in the Manning equation (equation 6.40c), we compute the values in table 6B8.2.

Table 6B8.2

Ψ (m)	0.50	1.00	1.50	2.00	2.50	3.00	3.50	3.78
R (m)	0.22	0.55	1.01	1.42	1.77	2.11	2.44	2.57
U (m/s)	0.727	1.335	2.000	2.507	2.903	3.264	3.596	3.723
Q (m^3/s)	2.42	21.4	61.9	118	187	272	374	432

Comparison of Estimates with Measured Values

Hicks and Mason (1991) provided measured values of R, U, and Q for this reach, so we can compare the two estimates with actual values, as shown in figure 6.26. The Chézy estimate, which uses only measured quantities (R, S, d_{84}) fits the measured values very closely except at the highest flow, while the Manning estimate of velocity is slightly too high (and depth too low) over most of the range. Recall though that the Manning estimate is based on a value of n_M determined by measurement in the reach; in many actual applications, such measurements would not be available, and we would be forced to estimate n_M by other means (section 6.8.2), probably leading to greater error.

In this example, the Chézy relation appears to give better results than the Manning relation.

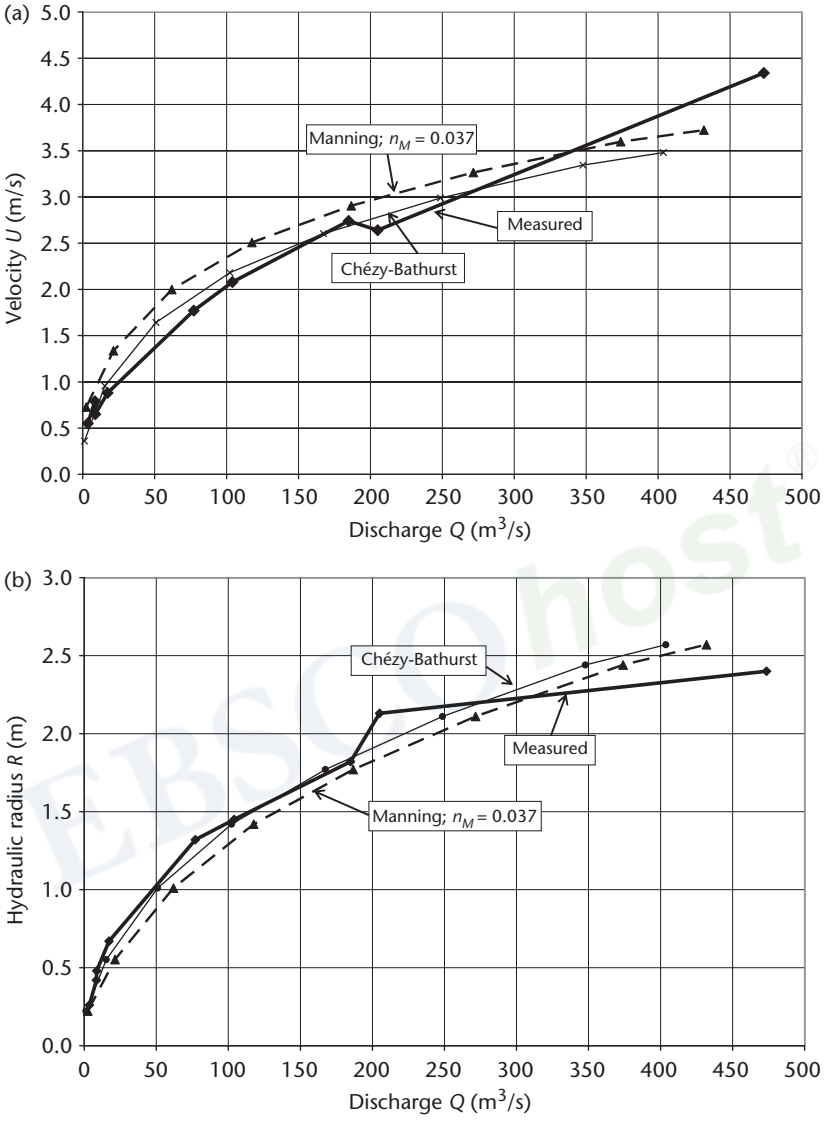

Figure 6.26 Comparison of estimated and actual hydraulic relations for the Hutt River cross section shown in figures 6.24 and 6.25. (a) Velocity–discharge relation. (b) Hydraulic radius (depth)–discharge relation. Heavy lines are measured; lighter solid line is calculated via Chézy equation with Bathurst (1993) resistance relation for gravel-bed streams (equation 6.27); dashed line is calculated via Manning equation using measured value of $n_M = 0.037$.

BOX 6.9 Slope-Area Computations, South Beaverdam Creek Near Dewy Rose, Georgia

A peak flood on 26 November 1957 left high water marks in a reach of South Beaverdam Creek near Dewy Rose, Georgia. The peak flood discharge was measured at $Q = 23.2$ m^3/s. The cross-sectional area, width, average depth, hydraulic radius, wetted perimeter, and water-surface slope defined by these high-water marks were surveyed by Barnes (1967) at five cross sections and are summarized in table 6B9.1.

Table 6B9.1

Section, i	A_i (m^2)	W_i (m)	Y_i (m)	R_i (m)	P_{wi} (m)	ΔX_i (m)	ΔZ_i (m)	$S_{Si} = \lvert\Delta Z_i\rvert/\Delta X_i$
0	24.9	21.6	1.16	1.10	22.6			
1	26.8	17.1	1.55	1.52	17.7	21.6	0.043	0.00197
2	25.8	18.0	1.43	1.32	19.5	20.1	0.037	0.00182
3	26.1	18.0	1.46	1.34	19.4	24.7	0.040	0.00161
4	24.2	17.7	1.37	1.26	19.2	19.5	0.018	0.00094
Average	$A =$	$W =$	$Y =$	$R =$	$P_W =$	$\Delta X =$	$\Delta Z =$	$S_S = 0.00160$
or sum	25.6	18.5	1.40	1.31	19.7	85.9	0.137	

To illustrate slope-area computations, we assume the discharge is unknown and apply three approaches that could be used to estimate a past flood discharge from high-water marks.

Standard Approach

This is the method described in section 6.8.2. We first assume we do not have a resistance determined by measurement in the reach. Table 6B9.2 gives the values of the quantities that are summed in equation 6.39c.

Table 6B9.2

Section, i	$A_i \cdot S_{Si} \cdot \Delta X_i$ (m^3)	$A_i \cdot \Delta X_i$ (m^3)	$P_{wi} \cdot \Delta X_i$ (m^3)
1	1.143	579	382
2	0.945	520	393
3	1.035	645	480
4	0.442	472	375
Sum	3.465	2216	1630

The channel bed "consists of sand about 1 ft deep over clay and rock. Banks are irregular with trees and bushes growing down to the low water line" Barnes (1967, p. 142). Because this is a sand-bed reach, we estimate Ω via equation 6.25 assuming $Y = R$ and $y_r = d_{84} = 0.002$ m (the upper limit for sand), and compute

$$\Omega = 0.400 \cdot \left[-\ln\left(\frac{0.002}{11 \cdot 1.31}\right)\right]^{-1} = 0.045.$$

Substituting the appropriate values into equation 6.48 gives

$$Q = \frac{9.81^{1/2} \cdot [3.465]^{1/2} \cdot 2216}{0.045 \cdot 85.9 \cdot [1630]^{1/2}} = 82.8 \text{ m}^3/\text{s}$$

as our estimate of peak discharge.

This estimate is several times too high. Thus, it appears that we severely underestimated the resistance using equation 6.25. Some of the "excess" resistance probably comes from the bank vegetation that extended into the flow, and some may be due to the development of ripples or dunes on the sand bed. Perhaps we could have come up with a better estimate using another of the approaches of section 6.8.2, or had accounted for effects of bedforms on the resistance (see section 6.6.4.2).

A better approach would be to determine the reach resistance via measurement before applying equation 6.48. On the day after the 26 November flood, when the flow was $Q = 6.26$ m^3/s, Barnes (1967) surveyed the same cross sections and obtained the values in table 6B9.3.

Table 6B9.3

Section, i	A_i (m^2)	R_i (m)	P_{wi} (m)	ΔX_i(m)	$\lvert\Delta Z_i\rvert$(m)	$S_{Si} = \lvert\Delta Z_i\rvert / \Delta X_i$
0	8.5	0.62	13.7			
1	11.9	0.82	14.5	21.6	0.034	0.00155
2	10.0	0.61	16.5	20.1	0.030	0.00152
3	10.0	0.60	16.6	24.7	0.024	0.00099
4	9.4	0.62	15.1	19.5	0.043	0.00219
Average or sum	$A = 9.96$	$R = 0.65$	$P_w = 15.3$	$\Delta X = 85.9$	$\lvert\Delta Z\rvert = 0.131$	$S_S = 0.00153$

We want to determine the value of Ω for this flow and use that value to estimate the flood peak on 26 November 1957. Table 6B9.4 gives the values of the quantities that are summed in equation 6.39c.

Table 6B9.4

Section, i	$A_i \cdot S_{Si} \cdot \Delta X_i$ (m^3)	$A_i \cdot \Delta X_i$ (m^3)	$P_{wi} \cdot \Delta X_i$ (m^3)
1	0.399	258	314
2	0.306	202	331
3	0.245	248	411
4	0.401	183	295
Sum	1.351	891	1351

Substituting the appropriate values into equation 6.39c yields

$$\Omega = \frac{9.81^{1/2} \cdot [1.351]^{1/2} \cdot 891}{6.26 \cdot 85.9 \cdot [1351]^{1/2}} = 0.164.$$

(*Continued*)

BOX 6.9 *Continued*

Thus, the measured reach resistance is several times higher than that based on equation 6.25. Finally, we use this measured value of Ω to estimate the peak discharge of 26 November 1957 via equation 6.48:

$$Q = \frac{9.81^{1/2} \cdot [3.465]^{1/2} \cdot 2216}{0.164 \cdot 85.9 \cdot [1630]^{1/2}} = 22.7 \text{ m}^3/\text{s}$$

The value of Q estimated using the Ω value measured in the reach is within 2% of the actual value.

Application of General Statistically Derived Relation

It is of interest to see how well the statistically developed "modified Manning" equation (equation 6.47) does in estimating the peak flood discharge from the high-water marks. Using values from table 6B9.1, that equation gives

$$Q = 7.14 \cdot 18.5 \cdot 1.40^{5/3} \cdot 0.00160^{1/3} = 27.1 \text{ m}^3/\text{s}.$$

The estimate for this case is quite good, about 17% higher than actual. The Froude number for this flow can be calculated from data in table 6B9.1:

$$Fr = \frac{U}{(g \cdot Y)^{1/2}} = \frac{Q/A}{(g \cdot Y)^{1/2}} = \frac{23.2/25.6}{(9.81 \cdot 1.40)^{1/2}} = 0.24$$

This value is in the range where equation 6.47 was found to give generally good predictions.

Application of Relation Developed from Dimensional Analysis

It is also of interest to see how well equation 4.74, developed by dimensional analysis and measurement data from New Zealand rivers, does in predicting the flood-peak discharge. Recall that that relation, written in terms of discharge, is

$$Q = 1.84 \cdot \left(\frac{Y}{y_r}\right)^{0.704} \cdot g^{1/2} \cdot W \cdot Y^{3/2} \cdot S_0^{1/2}, \; Y/y_r \leq 10; \qquad \text{(6B9.1a)}$$

$$Q = 9.51 \cdot g^{1/2} \cdot W \cdot Y^{3/2} \cdot S_0^{1/2}, \; Y/y_r > 10. \qquad \text{(6B9.1b)}$$

Since $y_r = 0.002$ m, $Y/y_r > 10$, and we use equation 6B9.1b with data from table 6B9.1:

$$Q = 9.51 \cdot 9.81^{1/2} \cdot 18.5 \cdot 1.40^{3/2} \cdot 0.00160^{1/2} = 36.5 \text{ m}^3/\text{s}$$

This estimate is 57% greater than actual, suggesting that equation 4.74 is not sufficiently precise to use for prediction (note the scatter in figure 4.14).

Longitudinal-profile irregularity: At high flows, the pool/riffle alteration tends to become submerged, tending to decrease resistance at higher flows (figure 6.11c).

Vegetation: Resistance may decrease at higher flows because flexible vegetation is bent further or because low vegetation becomes more submerged, or increase because more of the flow encounters bank and floodplain vegetation.

Surface stability: Resistance may increase at higher flows due to surface irregularities, particularly at bends or abrupt obstructions.

Sediment: In sand-bed streams, bedforms may be different at high flows than when flow is measured, leading to higher or lower resistance (figure 6.20).

Ice: During breakup of an ice cover, there may be large and unknown differences in resistance between the time of a high flow and when reach resistance is measured.

6.11 Summary

The standard approach to open-channel flow resistance is usually presented in terms of the Manning equation, with focus on determining appropriate values of Manning's n_M in various applications. However, the Manning equation was not derived from first principles, nor was it established by rigorous statistical analysis. Thus, this chapter has explored the fundamentals and practical aspects of resistance via the Chézy equation, which is derived from straightforward macroscopic force-balance considerations. This approach is consistent with fundamental fluid-mechanics principles:

- The Chézy derivation incorporates assumptions consistent with the models of turbulence presented in section 3.3.4 .
- Formulating the resistance as the dimensionless quantity Ω allows us to consider the subject in a way that is consistent with theoretical and observational approaches that are applicable in a wide range of fluid-mechanics contexts (summarized by the Moody diagram, figure 6.8).
- At least for the simplest flow situations, resistance can be related to measurable variables via physically based expressions for the velocity profile discussed in chapter 5 (equation 6.25).

As noted at the beginning of this chapter, our goal has been to develop relations for computing the average velocity U in a channel reach given the reach geometry, material, and slope and the depth or discharge. We expressed this relation as

$$U = \Omega^{-1} \cdot u_* = \Omega^{-1} \cdot (g \cdot R \cdot S)^{1/2} \approx \Omega^{-1} \cdot (g \cdot Y \cdot S)^{1/2} \tag{6.49}$$

and explored the factors that control Ω. Following Rouse (1965) and Yen (2002), we can summarize these factors for quasi-uniform flows in natural channels:

$$\Omega = f_\Omega(Y/y_r, Re, Y/W, \boldsymbol{\Psi}, \boldsymbol{\zeta}, \boldsymbol{\Theta}, \boldsymbol{V}, Fr, \boldsymbol{\Sigma}, \boldsymbol{I}), \tag{6.50a}$$

where $\boldsymbol{\Psi}$ represents the effects of cross-section irregularities, $\boldsymbol{\zeta}$ the effects of planform irregularities, $\boldsymbol{\Theta}$ the effects of longitudinal-profile irregularities, $\boldsymbol{V}$ the effects of vegetation, $\boldsymbol{\Sigma}$ the effects of sediment transport, and $\boldsymbol{I}$ the effects of ice.

Considering only ice-free channels and noting that the effects of Y/W are generally minor in natural channels (figure 6.10), we can write

$$\boldsymbol{\Omega} \approx f_{\Omega}(Y/y_r, Re, \boldsymbol{\Psi}, \boldsymbol{\zeta}, \boldsymbol{\Theta}, \boldsymbol{V}, Fr, \boldsymbol{\Sigma}). \tag{6.50b}$$

Further simplification may be possible if we recall that the effects of cross-sectional variability $\boldsymbol{\Psi}$ and longitudinal variability $\boldsymbol{\Theta}$ are at least in part captured by the relative submergence Y/y_r, so that

$$\Omega \approx f_{\boldsymbol{\Omega}}(Y/y_r, Re, \boldsymbol{\zeta}, \boldsymbol{V}, Fr, \boldsymbol{\Sigma}). \tag{6.50c}$$

One barrier to using 6.50c to determine velocity via 6.49 is that Re, $\boldsymbol{\zeta}$, Fr, $\boldsymbol{\Sigma}$, and to some extent $\boldsymbol{V}$ all depend on velocity—so we are faced with a logical circularity. However, if we confine ourselves to fully rough flows in wide, reasonably straight channels at low to moderate Froude numbers and insignificant sediment transport, the problem becomes more tractable:

$$\Omega \approx f_{\Omega}(Y/y_r). \tag{6.50d}$$

Based on the P-vK law and the analyses in section 6.6, we can be reasonably confident that the form of this relation is given by

$$\Omega \approx \kappa \cdot \left[\ln\left(\frac{K_r \cdot Y}{y_r} \right) \right]^{-1}. \tag{6.51}$$

The standard form of this relation is the C-K equation, in which $\kappa = 0.400$ and $K_r = 11$. However, as we have seen in equations 6.27, 6.28, 6.30, and 6.32, the values of κ and K_r may vary from reach to reach—and maybe even for different flows in the same reach.

We saw in box 6.7 that the Chézy approach incorporating an appropriate resistance relation can provide good estimates of velocity-discharge and depth-discharge relations that can be used to solve practical problems.

Approaching resistance via the Chézy equation also provides a straightforward formula for computing reach resistance from field data (equation 6.39). This formula can be inverted to give a relation for estimating past flood discharges in slope-area computations (equation 6.48). However, we saw in box 6.9 that such estimates can be erroneous in the absence of appropriate resistance estimates.

Clearly, although we have learned much about the factors that determine reach resistance, there are still many uncertainties to be faced in obtaining reliable a priori and a posteriori resistance estimates for practical use and much need for additional research in this area.

7

Forces and Flow Classification

7.0 Introduction and Overview

The forces involved in open-channel flow are introduced in section 4.2.2.1. The goals of this chapter are 1) to develop expressions to evaluate the magnitudes of those forces at the macroscopic scale, 2) to examine the relative magnitudes of the various forces in natural channels and show how they change with the flow scale, and 3) to show that the Reynolds number (introduced in section 3.4.2) and the Froude number (introduced in section 6.2.2.2) can be interpreted in terms of force ratios. Understanding the relative magnitudes of forces provides a helpful perspective for developing quantitative solutions to practical problems.

Open-channel flows are induced by gradients of potential energy proportional to the sine of the water-surface slope (section 4.7). This chapter shows that the water-surface slope reflects the magnitude of the driving forces due to gravity and pressure. Once motion begins, frictional forces resisting the flow arise due to molecular viscosity and, usually, turbulence; these forces are increasing functions of velocity. In steady uniform flow, which was assumed in the developments of chapters 5 and 6, the gravitational driving force is balanced by the frictional forces, so there is no acceleration and no other forces are involved. However, in general, the forces affecting open-channel flows are not in balance, so the flow experiences convective acceleration (spatial change in velocity) and/or local acceleration (temporal change in velocity)—concepts introduced in section 4.2.1.2 at the "microscopic" scale (fluid elements).

In this chapter, as in chapters 5 and 6, we continue to analyze the flow on a macroscopic scale; that is, the physical relations are developed for the entire flow in a reach in an idealized channel rather than for a fluid element. We consider changes only in time and in one spatial dimension (the downstream direction), so the resulting equations are characterized as "one-dimensional."

The chapter begins by reviewing the forces that induce and oppose fluid motion in open channels and presenting the basic force-balance equations for various flow categories. Next we lay out the basic geometry of an idealized reach and then formulate quantitative expressions for the magnitudes of the various forces as functions of fluid properties and flow parameters. We also develop expressions for the convective and local accelerations so that we can ultimately formulate the complete macroscopic force-balance equation for one-dimensional open-channel flow.

Using data for a range of flows, we examine the typical values of each of the forces in natural streams and compare their magnitudes. We also compare the relative magnitudes of the forces as a function of scale, from small laboratory flumes to the Gulf Stream. This comparison provides guidance for identifying conditions under which the force balance may be simplified by omitting particular forces due to their relative insignificance. The chapter concludes by showing how the Reynolds and Froude numbers can be interpreted in terms of force ratios.

7.1 Force Classification and the Overall Force Balance

In this section we formulate the overall force-balance relations for flows of various categories. To simplify the development, these relations are formulated for the simple open-channel flow shown in figure 7.1: a wide rectangular channel ($Y = R$) with constant width ($W_1 = W_2 = W$) but spatially varying depth. At any instant, the reach contains a spatially constant discharge Q, so

$$Q = W \cdot Y_1 \cdot U_1 = W \cdot Y_2 \cdot U_2, \tag{7.1}$$

where Y_i is the average depth and U_i is the average velocity at section i.

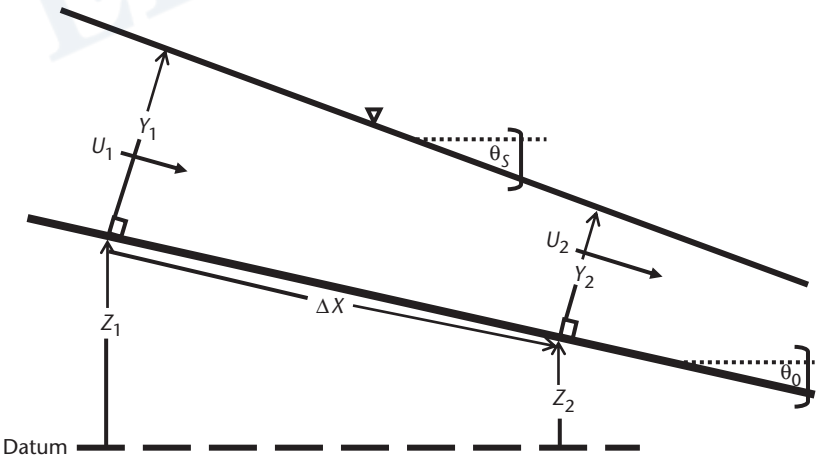

Figure 7.1 Definition diagram for deriving expressions to calculate force magnitudes for a nonuniform flow in a prismatic channel. Width and discharge are assumed constant.